An Overview of

ALICE

A Large Ion Collider Experiment

a Particle Detection setup at

LHC (Large Hadron Collider)

M. Ikram Shahzad

Introduction

- The idea of the atomic nature of matter had been presented as early as 5^{th} century B.C by the Greek philosophers. However such a conjecture was not subject to systematic experimental tests in the absence of appropriate scientific instrumentation and methodology.
- The experimental methods were popularized by the Arabs during 750 A.D to 1100 A.D but no attempt was made to correlate the experimental data in terms of theoretical models.
- The modern concept of atom was born in the early nineteenth century after the availability of data based on a number of chemical and physical observations.
- During the period of one hundred years between 1811 A.D to 1911 A.D the scientist's perception of the atom has been greatly modified. The final picture, as we know it now, is that an atom is the smallest part of an element which manifests its physical and chemical properties.
- The negatively charged part is in the form of an electron cloud which is distributed in a region with a radius of the order of 10^{-10} m. The positive part is concentrated in an extremely small region at the centre of the atom. The radius of this region is of the order of 10^{-15} m and it contains almost all the mass of the atom; thereby an enormous density of the order of 10^{17} kg/m^3.

Quarks

Makeup Matter

Mesons,   Baryons

2-quarks, 3 or more

Leptons

Makeup Matter

Electron, Muon, Tau

and their Neutrinos

Bosons

Force Carriers

Graviton

Photon

Gluon

W & Z

Higgs

A Partial List of Elementary Particles

Classification	Name	Symbol	Charge	Mass (MeV/c^2)	Life Time (second)
Photons		γ	0	0	∞
Leptons	Neutrino	ν_e, $\bar{\nu}_e$ ν_μ, $\bar{\nu}_\mu$ ν_τ, $\bar{\nu}_\tau$	0 0 0	$<7\text{x}10^{-6}$ < 0.27 < 31	∞ ∞ ∞
	Electron	$e^\pm$	±e	0.511	∞
	Muon	$\mu^\pm$	±e	105.7	$2.20\text{x}10^{-6}$
	Tau	$\tau^\pm$	±e	1784	$3.04\text{x}10^{-13}$
Mesons	Pion	$\pi^\pm$ π^0	±e 0	139.6 135.0	$2.60\text{x}10^{-8}$ $0.87\text{x}10^{-16}$
	Kaon	$K^\pm$ K^0, ($\bar{K}^0$)	±e 0	493.7 497.7	$1.24\text{x}10^{-8}$ $0.89\text{x}10^{-10}$
	D meson	$D^\pm$ D^0, ($\bar{D}^0$)	±e 0	1869 1865	$10.7\text{x}10^{-13}$ $4.3\text{x}10^{-13}$
Baryons	Proton	p, $\bar{p}$	±e	938.3	> 10^{39}
	Neutron	n, $\bar{n}$	0	939.6	896
	Lambda	Λ, $\bar{\Lambda}^0$	0	1116	$2.63\text{x}10^{-10}$
	Sigma	Σ^+, $\bar{\Sigma}^+$ Σ^0, $\bar{\Sigma}^0$ Σ^-, $\bar{\Sigma}^-$	±e 0 ±e	1189 1193 1197	$0.80\text{x}10^{-10}$ $7.40\text{x}10^{-10}$ $1.48\text{x}10^{-10}$
	Xi	Ξ^0, $\bar{\Xi}^0$ Ξ^+, $\bar{\Xi}^+$	0 ±e	1315 1321	$2.90\text{x}10^{-10}$ $1.64\text{x}10^{-10}$
	Omega	Ω^-, $\bar{\Omega}^+$	±e	1672	$0.82\text{x}10^{-10}$

Leptons

Name	Symbol	Charge	Mass (MeV/c²)
Electron	e^-	-e	0.511
Positron	e^+	+e	0.511
Muon	μ^-	-e	105.7
Positive muon	μ^+	+e	105.7
Tau	τ^-	-e	1784
Positive tau	τ^+	+e	1784
Electron neutrino	ν_e	0	$<7\text{x}10^{-6}$
Electron antineutrino	$\bar{\nu}_e$	0	$<7\text{x}10^{-6}$
Muon neutrino	ν_μ	0	< 0.27
Muon antineutrino	$\bar{\nu}_\mu$	0	< 0.27
Tau neutrino	ν_τ	0	< 31
Tau antineutrino	$\bar{\nu}_\tau$	0	< 31

Quarks

Quark	Symbol	Charge	Mass (MeV)
Up	u	+2/3	360
Down	d	-1/3	360
Charm	c	+2/3	1500
Strange	s	-1/3	540
Top	t	+2/3	174000
Bottom	b	-1/3	5000

Antiquarks

Quark	Symbol	Charge	Mass (MeV)
Antiup	$\bar{u}$	-2/3	360
Antidown	$\bar{d}$	+1/3	360
Anticharm	$\bar{c}$	-2/3	1500
Antistrange	$\bar{s}$	+1/3	540
Antitop	$\bar{t}$	-2/3	174000
Antibottom	$\bar{b}$	+1/3	5000

Mesons

(Particles that Makeup Matter)

Name	Symbol	Makeup	Mass (MeV/c^2)	Life Time (second)
Pion	$\pi^\pm$ π^0	$u\bar{d}$, $d\bar{u}$ $(u\bar{u}+d\bar{d})/\sqrt{2}$	139.6 135.0	2.60×10^{-8} 0.87×10^{-16}
Kaon	$K^\pm$ K^0, ($\bar{K}^0$)	$u\bar{s}$, $s\bar{u}$ $d\bar{s}$, $s\bar{d}$	493.7 497.7	1.24×10^{-8} 0.89×10^{-10}
D meson	$D^\pm$ D^0, ($\bar{D}^0$) $D_s^\pm$	$c\bar{d}$ $c\bar{u}$, $u\bar{c}$ $c\bar{s}$	1869 1865 1969	10.7×10^{-13} 4.3×10^{-13} 4.7×10^{-13}
Psi/J	J/ψ	$c\bar{c}$	3097	0.8×10^{-20}
upsilon	ε	$b\bar{b}$	9460	1.3×10^{-20}
Eta	η^0 $\eta^{0'}$	$(u\bar{u}-d\bar{d})/\sqrt{2}$ $s\bar{s}$	548.8 958	$<10^{-18}$
Rho	$\rho^\pm$ ρ^0	$u\bar{d}$, $d\bar{u}$ $u\bar{u}$, $d\bar{d}$	770 770	0.4×10^{-23}
Phi	ϕ	$s\bar{s}$	1020	20×10^{-23}
Omega	ω^0	$u\bar{u}$, $d\bar{d}$	782	0.8×10^{-22}

Baryons

(Particles that Makeup Matter)

Name	Symbol	Makeup	Mass (MeV/c^2)	Life Time (second)
Proton	p	uud	938.3	> 10^{39}
Neutron	n	ddu	939.6	896
Lambda	Λ^0	uds	1116	2.63×10^{-10}
	$\Lambda^+{}_c$	udc	2285	2.0×10^{-13}
	$\Lambda^0{}_b$	udb	5624	1.2×10^{-12}
Sigma	Σ^+	uus	1189	0.80×10^{-10}
	Σ^0	uds	1193	7.40×10^{-10}
	Σ^-	dds	1197	1.48×10^{-10}
	$\Sigma^+{}_b$	uub		
	$\Sigma^-{}_b$	ddb		
Delta	Δ^{++}	uuu	1232	0.63×10^{-23}
	Δ^+	uud		
	Δ^0	udd		
	Δ^-	ddd		
Xi	Ξ^0	uss	1315	2.90×10^{-10}
	Ξ^-	dss	1321	1.64×10^{-10}
	$\Xi^+{}_c$	usc	2466	4.4×10^{-13}
	$\Xi^0{}_c$	dsc	2472	1.1×10^{-13}
	$\Xi^-{}_c$	dsb	5792	1.42×10^{-12}
Omega	Ω^-	sss	1672	0.82×10^{-10}
	$\Omega^0{}_c$	ssc	2698	7×10^{-14}
Pentaquark	Θ^+	uddu s	1540	

Bosons

(Particles that Transmit Forces)

Name	Spin	Charge	Mass (GeV)	Observed
Graviton	2	0	0	Not Yet
Photon	1	0	0	Yes
Gluon	1	0	0	Indirectly (not observed singly)
W^+	1	+1	80	Yes
W^-	1	-1	80	Yes
Z^0	1	0	91	Yes
Higgs	0	0	>78	Not Yet

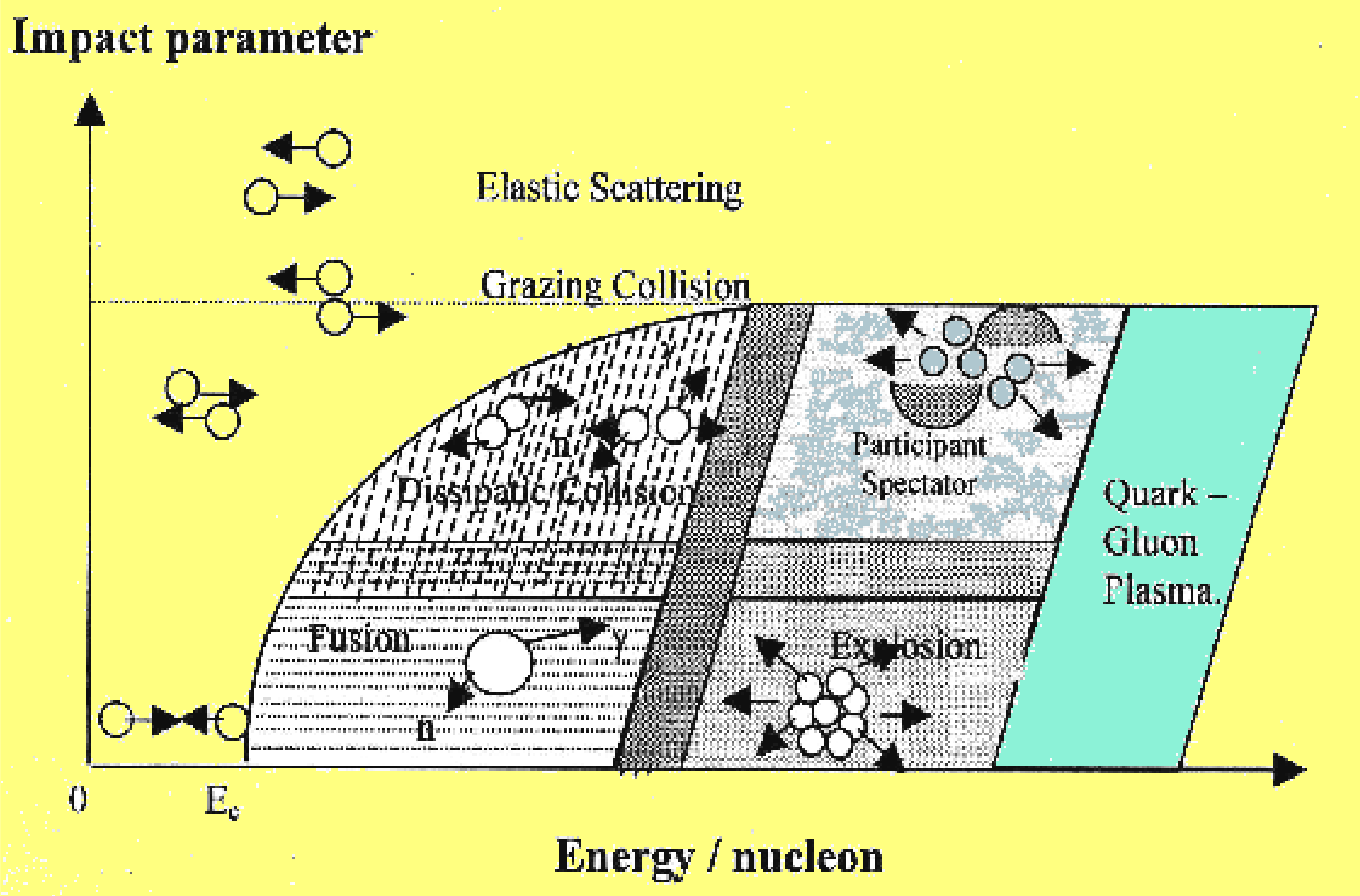

Different reaction regimes in terms of incident energy and impact parameter

Heavy Ions Physics

QCD Thermodynamics:

- **Strongly interacting matter at extreme energy density and thermodynamical behaviour at energy of deconfinement thresholds-the QGP-fundamental symmetries are explicit**
- **High density; transition of hadronic matter to QGP (10^{-5} s after Big Bang, neutron star)**
- **Parameters related to QGP; the energy density, the size of the system, the lifetime of the system, relaxation time**

LHC Experiments

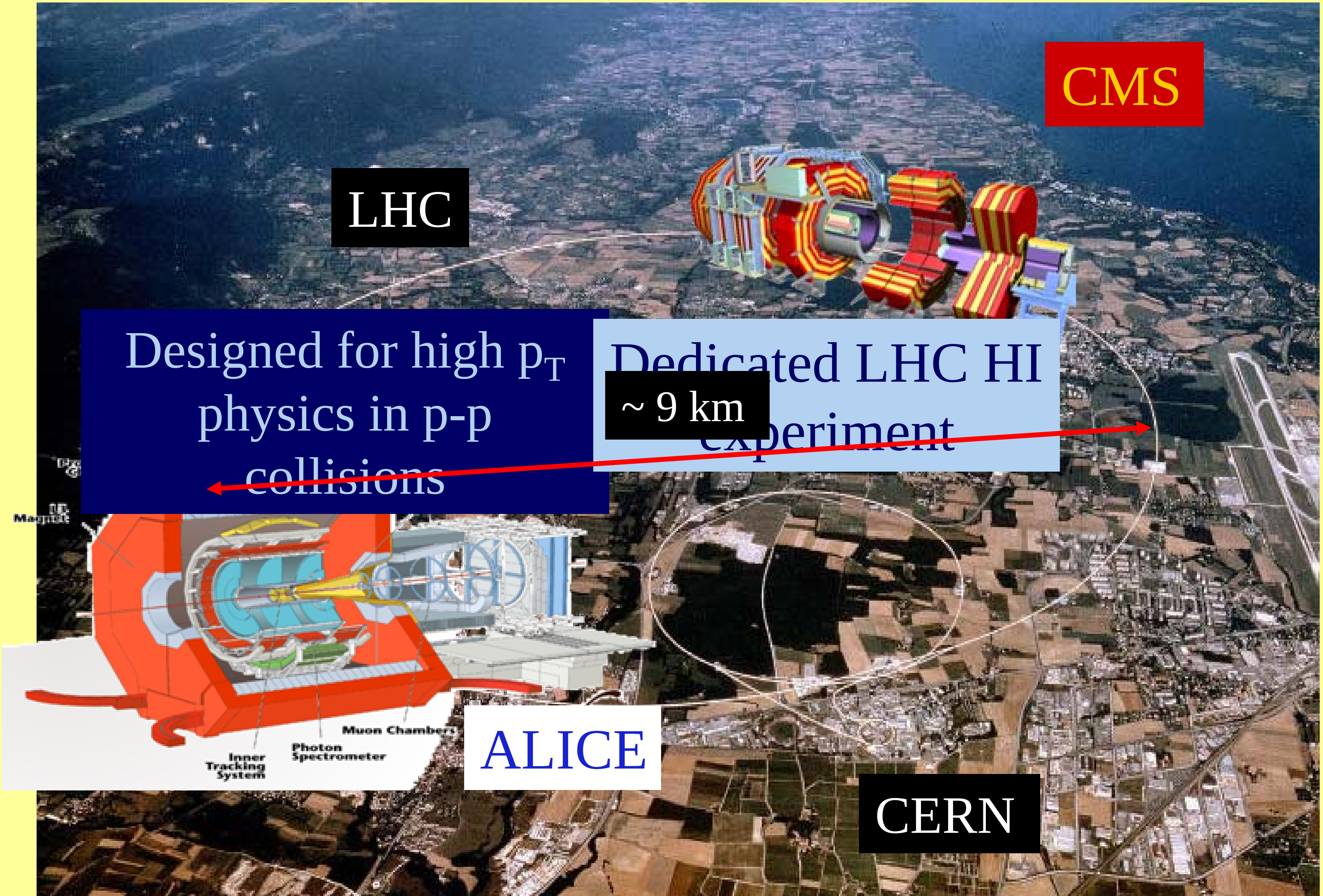

LHC experiments at CERN

- **ALICE (A Large Ion Collider Experiment)**
- **Specially optimized to study heavy ion collisions particularly Pb-Pb nuclei at the center-of-mass energy of 5.5 ATeV (collision energy of 1150 TeV). The resulting temperature and density are expected to be large enough to generate a quark-gluon plasma (a state of matter wherein quarks and gluons are deconfined).**
- **Using heavy ion collisions for attaining the high energy densities (1-100 GeV/fm^3) over large volume and long time scale will investigate equilibrium as well as non-equilibrium physics of strong interacting matter.**
- **ATLAS** (A Toroidal LHC ППpratuS)
- **CMS** (Compact Muon Solenoid)
- **LHCb** (LHC-beauty)
- **LHCf** (LHC-forward)
- **TOTEM** (Total Cross Section, Elastic Scattering and Diffraction Dissociation)

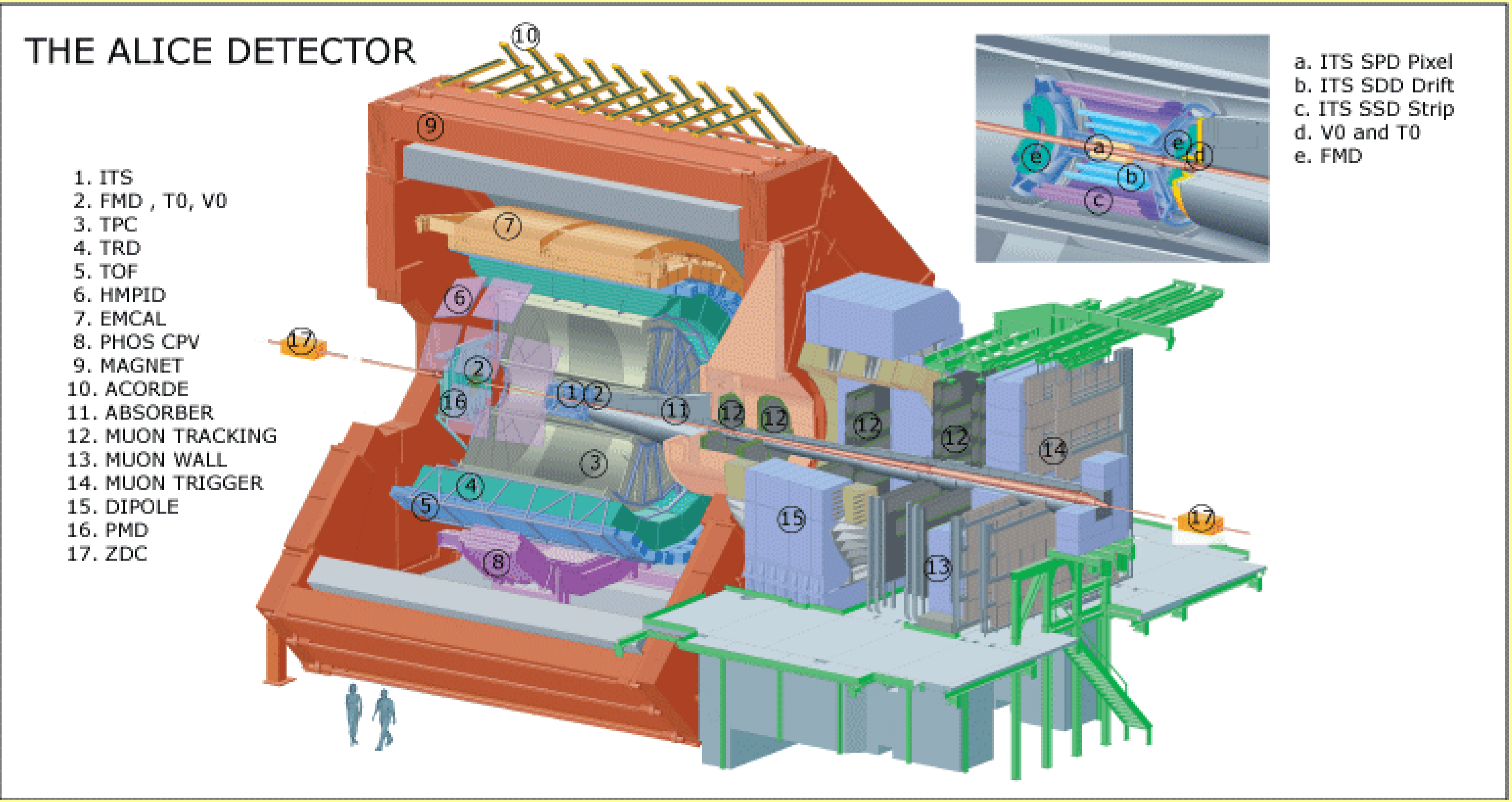
THE ALICE DETECTOR
1. ITS
2. FMD , T0, V0
3. TPC
4. TRD
5. TOF
6. HMPID
7. EMCAL
8. PHOS CPV
9. MAGNET
10. ACORDE
11. ABSORBER
12. MUON TRACKING
13. MUON WALL
14. MUON TRIGGER
15. DIPOLE
16. PMD
17. ZDC
a. ITS SPD Pixel
b. ITS SDD Drift
c. ITS SSD Strip
d. V0 and T0
e. FMD

Heavy Ions Physics with ALICE

- Initial Conditions:

➢ **Global Event Features for dynamics of nuclear collisions, measuring the number of colliding nucleons and information on the energy density obtained to understand the kinematical parameters of nuclear reaction i.e. the impact parameters, overlap of projectile-target, number of constituents participating in the interaction, number of exit particles etc. The data measured using Forward Zero Degree Calorimeter of ALICE will be used. Analysis of the reactions on event-by-event basis will be carried out using the data of observables measured with the help of the Forward Multiplicity Detector (FMD).**

- QGP:

✓ Open Charm production will probe the parton kinematics

✓ Prompt Photons reveal the characteristic thermal radiation from the plasma

✓ High Transverse Momentum Hadron's cross-section is sensitive to the energy loss of the parton in the plasma

✓ J/ψ production probe the deconfinement

Heavy Ions Physics with ALICE

- Phase Transition:
- **Strangeness Production is sensitive to the large s quark density expected from chiral-symmetry restoration in the plasma (light meason spectra)**
- **Multiplicity Fluctuations are a signature for the critical phenomena at the onset of a phase transition**
- **Particle Interferometry measures the expansion time in the mixed phase**
- Hadronic Matter:
- **Particle Ratios**, Transverse Momentum Distribution and Resonance Line-Shape Parameters are all sensitive to the dynamic evolution of the hadronic phase
- **Interfaerometry** allows measurement of the freez -out radius of the hadronic fireball

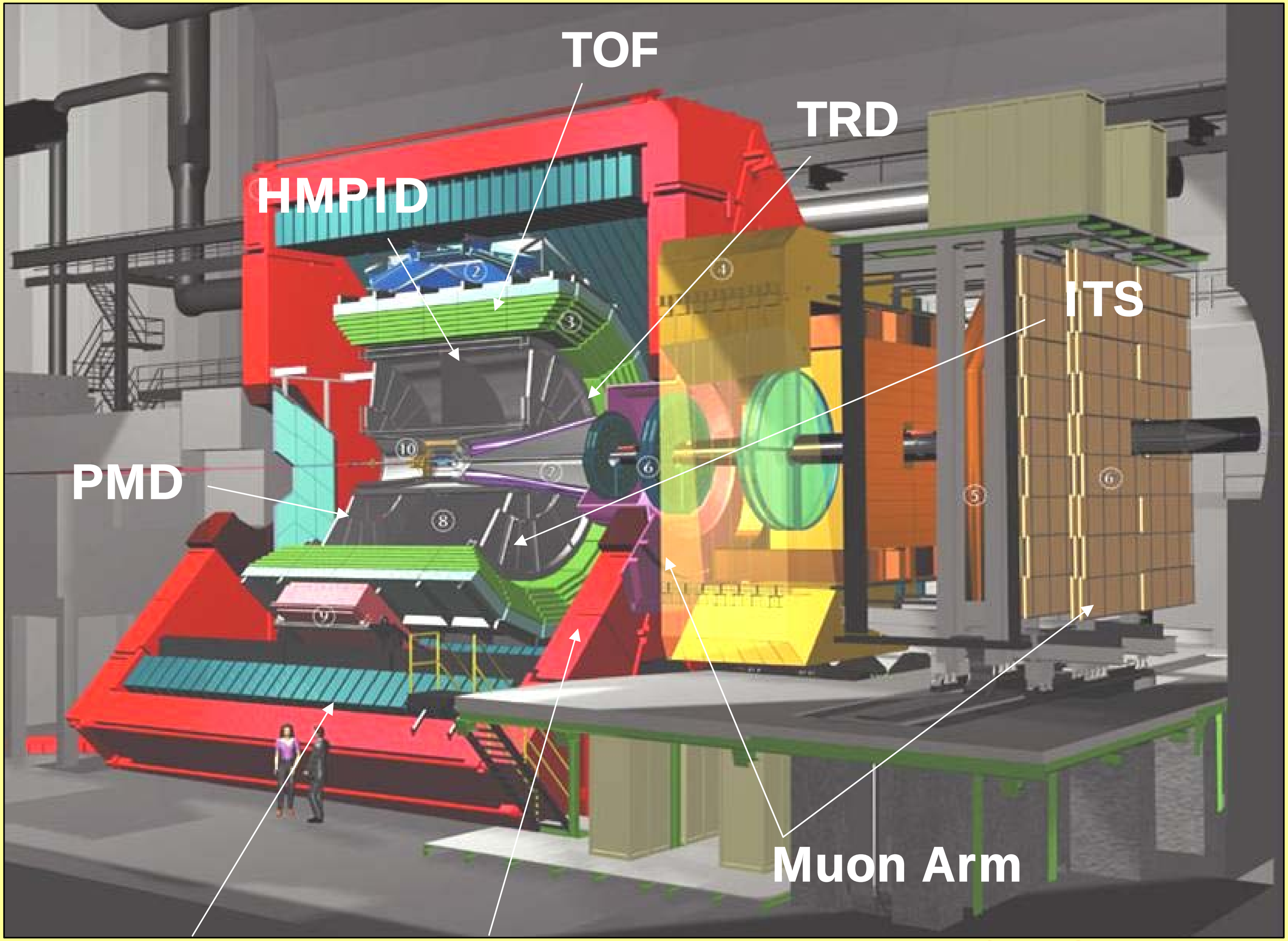

ALICE Set-up

Initial Conditions:

First one needs to know the initial conditions, namely how powerful the collision was: this is done by measuring the remnants of the colliding nuclei in detectors made of high density materials located about 110 meters on both sides of ALICE (the ZDCs) and by measuring with the FMD, V0 and T0 the number of particles produced in the collision and their spatial distribution. T0 also measures with high precision the time when the event takes place.

Tracking particles:

An ensemble of cylindrical detectors (from inside out: ITS (SPD, SDD, SSD), TPC, TRD) measures at many points (over 100 just the TPC) the passage of each particle carrying an electric charge, so that its trajectory is precisely known. The ALICE tracking detectors are embedded in a magnetic field bending the trajectories of the particles: from the curvature of the tracks one can find their momentum. The ITS is so precise that particles which are generated by the decay of other particles with a very short life time can be identified by seeing that they do not originate from the point where the interaction has taken place (the “vertex” of the event) but rather from a point at a distance of as small as a tenth of a millimeter

Particles Identification:

We also wants to know the identity of each particle, whether it is an electron, or a proton, a kaon or a pion. In addition to the information given by ITS and TPC, more specialized detectors are needed. The TOF measures, with a precision better than a tenth of a billionth of a second, the time that each particle takes to travel from the vertex to reach it, so that, one can measure its speed. The HMPID measures the faint light patterns generated by fast particles and the TRD measures the special radiation very fast particles emit when crossing different materials, thus allowing to identify electrons. Muons are measured by exploiting the fact that they penetrate matter more easily than most of other particles, therefore, in the forward region a very thick and complex absorber stops all other particles and muons are measured by a dedicated set of detectors called the muon spectrometer

Detection of Photons:

The photons, like the light emitted from a hot object, tell us about the temperature of the system. To measure them, special detectors are used The crystals of the PHOS, which are as dense as lead and as transparent as glass are used to measure them with fantastic precision in a limited region, while the PMD and in particular the EMCalorimeter (EMCal) are to measure them over a very wide area. The EMCal will also measure groups of close particles (called “jets”) which have a memory of the early phases of the event.

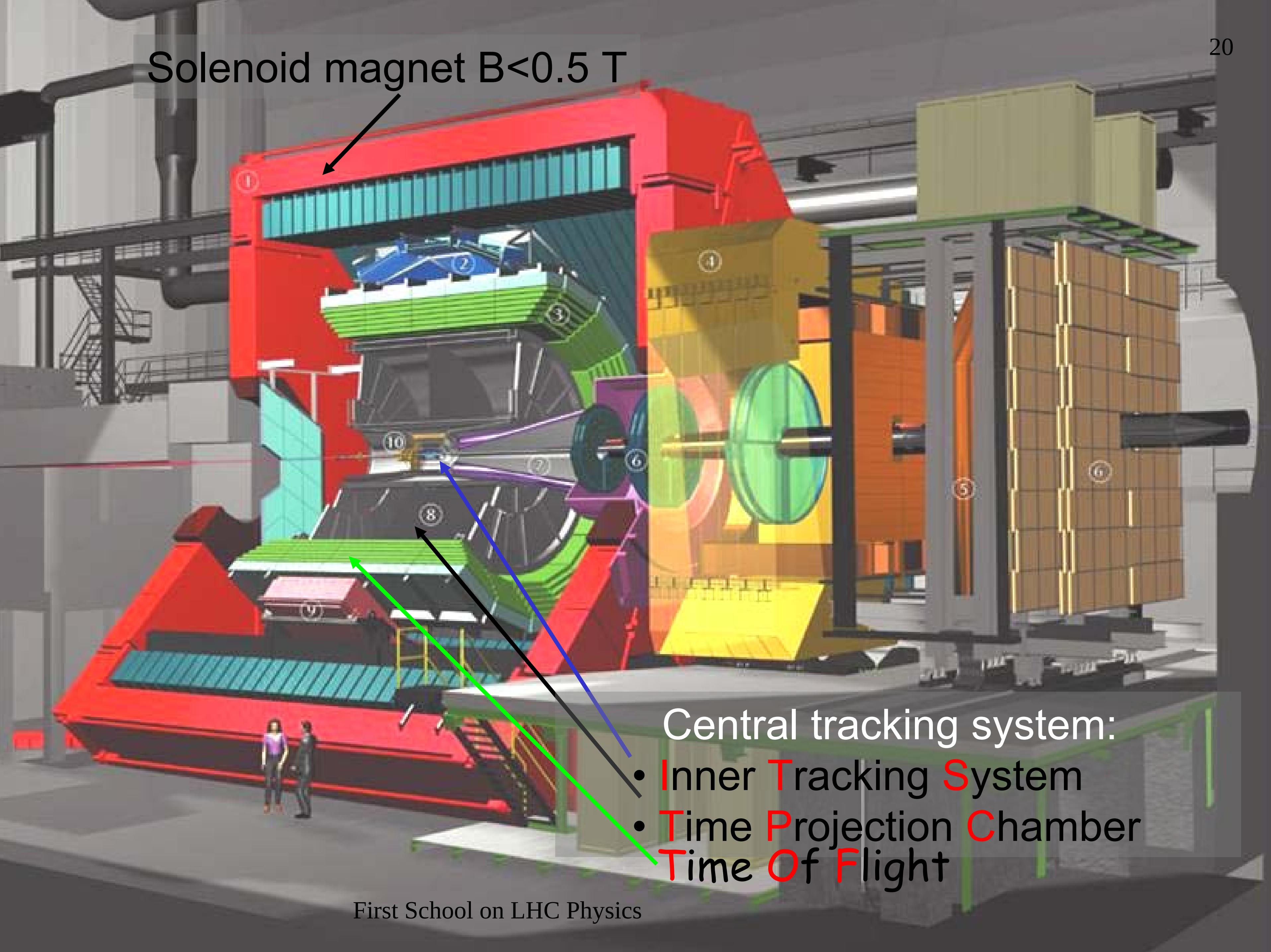

Solenoid magnet B<0.5 T

Central tracking system:

- Inner Tracking System
- Time Projection Chamber

Time Of Flight

Inner Tracking System (ITS)

ITS consists of six cylindrical layers of silicon detectors, located at radii, r = 4, 7, 15, 24, 39 and 44 cm. It covers the rapidity range of $|\eta| < 0.9$ for all vertices located within the length of the interaction diamond ($\pm 1\sigma$), i.e. 10.6 cm along the beam direction. The number, position and segmentation of the layers are optimized for efficient track finding and high impact-parameter resolution. In particular, the outer radius is determined by the necessity to match tracks with those from the TPC, and the inner radius is the minimum allowed by the radius of the beam pipe (3 cm). The first layer has a more extended coverage ($|\eta| < 1.98$) to provide, together with the FMD, a continuous coverage in rapidity for the measurement of charged-particles multiplicity.

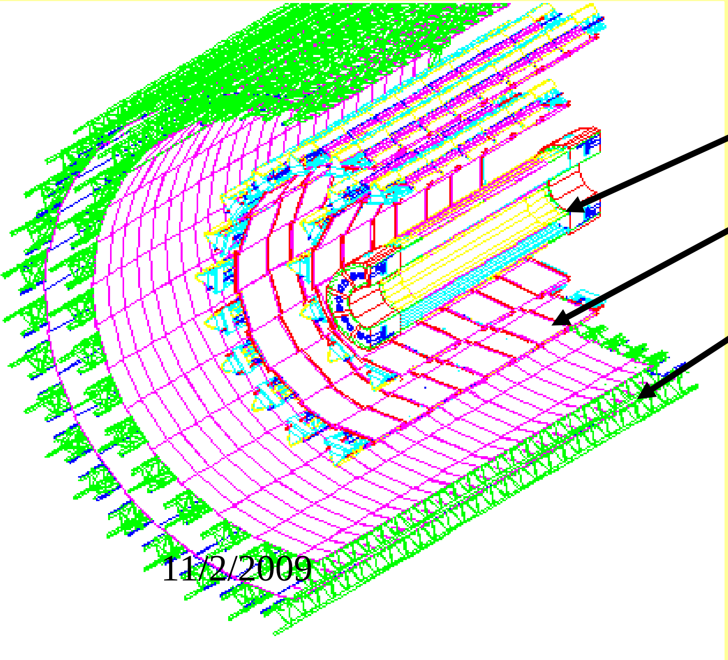

Three Tecnhnologies:

SPD - Silicon Pixel

SDD - Silicon Drift

SSD - Silicon Strip

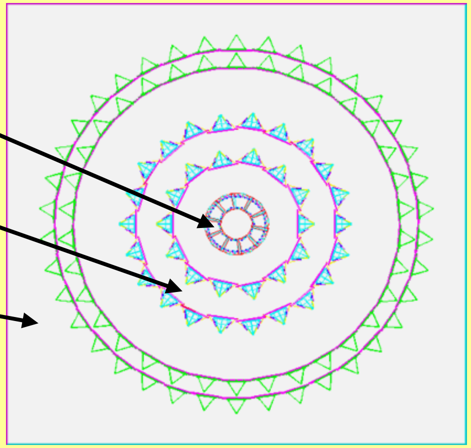

Inner Tracking System (ITS)

The tasks of the ITS

- to localize the primary vertex with a resolution better than 100 μm;
- to reconstruct the secondary vertices (5μm in beam direction and 25 μm in transverse plane) from decays of hyperons and D and B mesons;
- to track and identify particles with momentum below 100 MeV;
- to improve the momentum and angle resolution for the high-p_t (>0.2 Gev/c, 100%; >1 GeV/c' 90%) particles which also traverse the TPC;
- to reconstruct, albeit with limited momentum resolution (0.7%; 1 GeV/c), particles traversing dead regions of the TPC.

The ITS contributes to the global tracking of ALICE by improving the momentum and angle resolution obtained by the TPC. In addition to the improved momentum resolution, the ITS provides an excellent double-hit resolution enabling the separation of tracks with close momenta.

Dimensions of the ITS detectors (active areas).

Layer	Type	r (cm)	$\pm z$ (cm)	Area (m^2)	Ladders	Lad./stave	Det./ladder	Channels
1	Pixel	3.9	14.1	0.07	80	4	1	3 276 800
2	Pixel	7.6	14.1	0.14	160	4	1	6 553 600
3	Drift	15.0	22.2	0.42	14	–	6	43 008
4	Drift	23.9	29.7	0.89	22	–	8	90 112
5	Strip	37.8/38.4	43.1	2.09	34	–	22	1 148 928
6	Strip	42.8/43.4	48.9	2.68	38	–	25	1 459 200
Total area				6.28				

Silicon Pixel Detectors (SPD)

Two innermost Layers of ITS, for the determination of position of primary vertex and for measurement of impact parameter of secondary tracks originating from the weak decays of strange and beauty particles. Tacking in $|\eta| < 0.9$

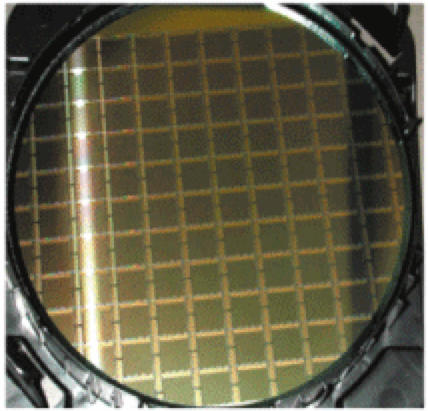

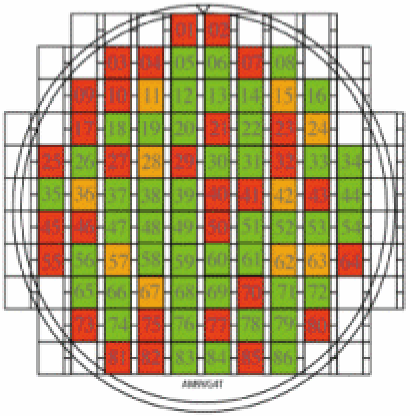

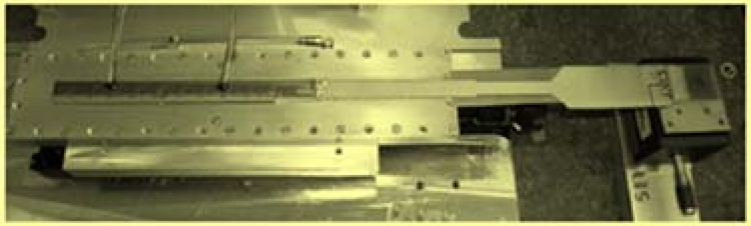

A 144 mm long half-stave

A prototype Multi-Chip-Module

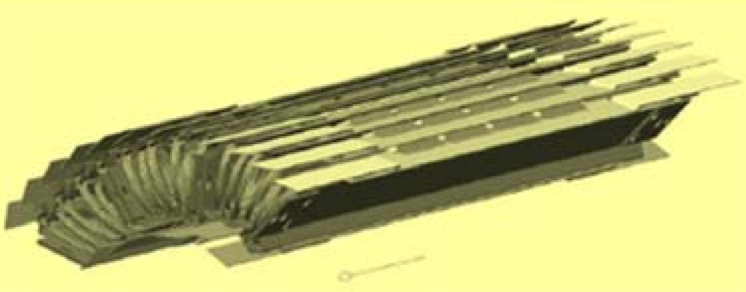

Carbon fiber support sector assembly

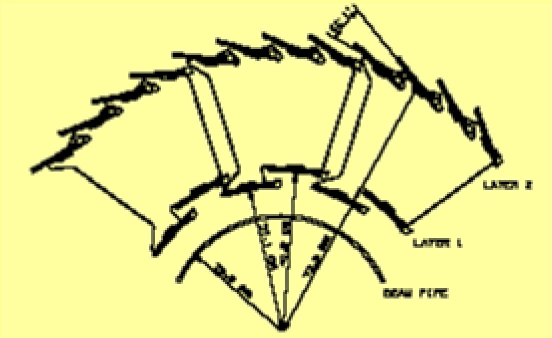

Carbon fiber support of the Si-pixel stave

Silicon Drift Detectors (SDD)

The SDD is equipd with the two intermediate layers of the ITS, where the charged particle density is expected to reach up to 7 cm^{-2}. They have a very good multitrack capability and provide two out of the four dE/dx samples needed for the ITS particle identification.

The SDDs are mounted on linear structures called ladders. There are 14 ladders with six detectors on layer 3, and 22 ladders with eight detectors on layer 4. Detectors and ladders are assembled to have an overlap of the sensitive areas larger than 580 μm in both rφ and z directions. This ensures full angular coverage for vertices located in the interaction diamond, ±σ = 10.6 cm, and for 35 MeV/c < p_t < 2.8 GeV/c.

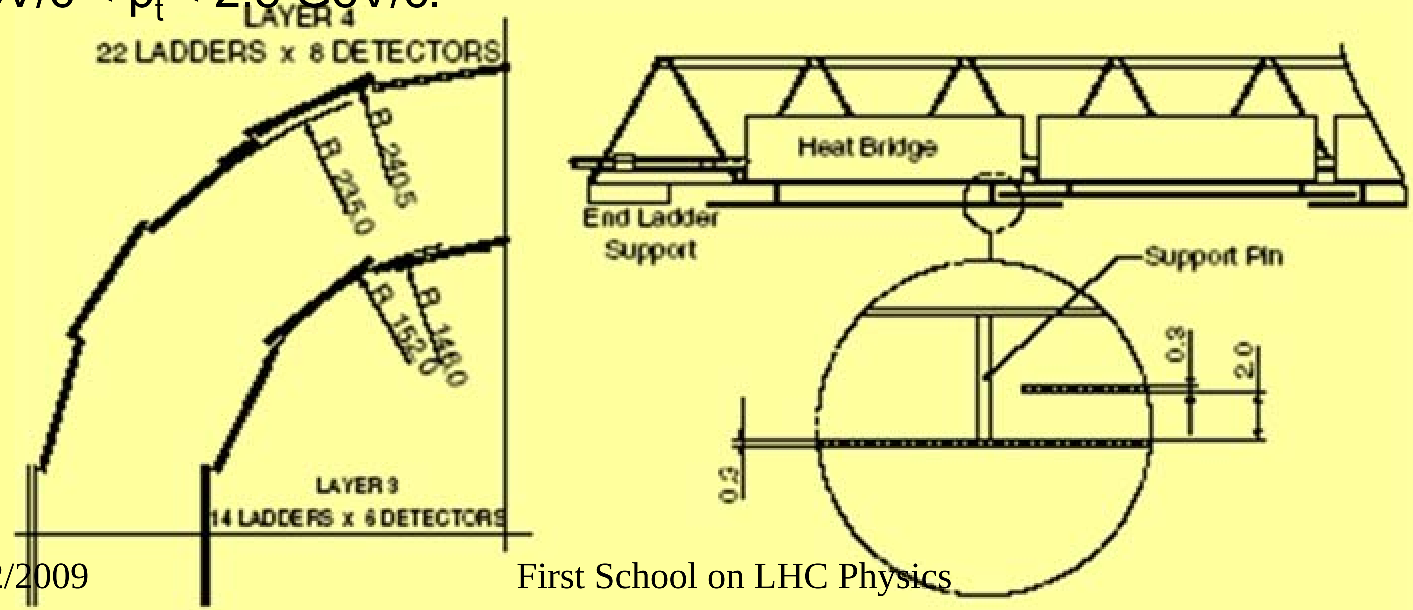

The SDDs are mounted at different radii in both rz and rφ planes to obtain the full coverage in the acceptance region.

Silicon Drift Detectors (SDD)

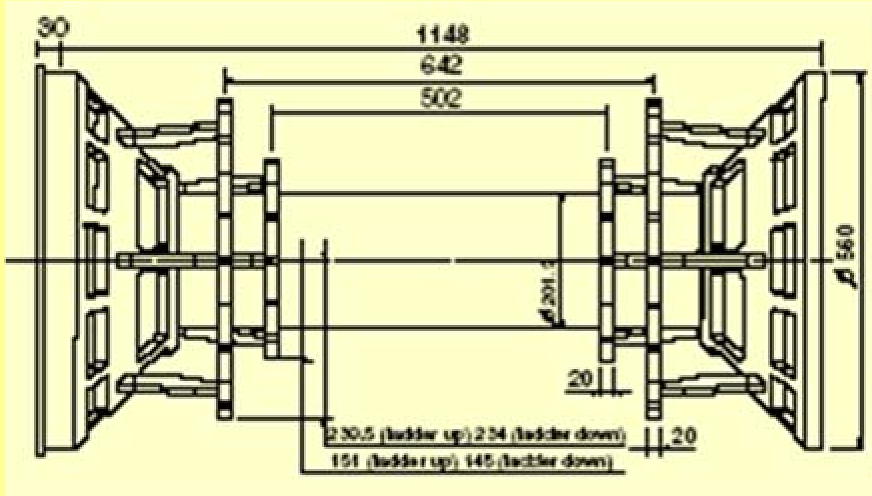

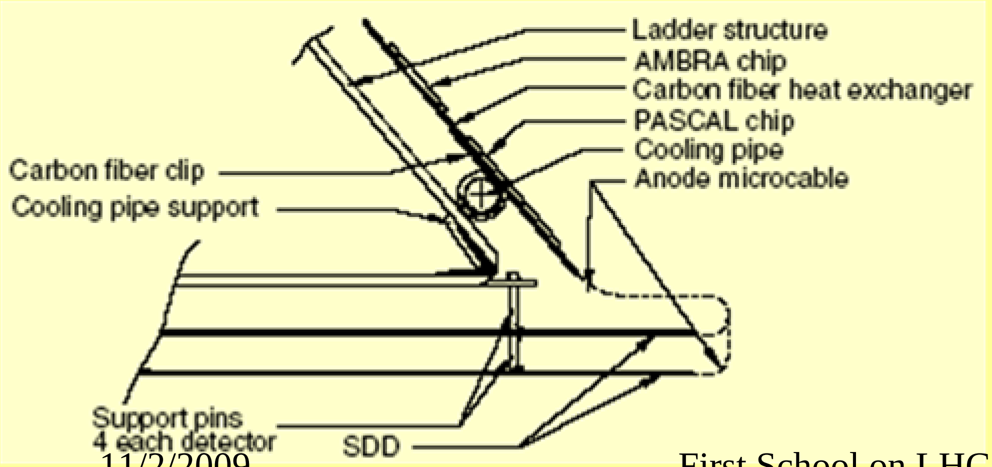

Sensitive area	$70.17 \times 75.26\ \mathrm{mm}^2$
Total area	$72.50 \times 87.59\ \mathrm{mm}^2$
Collection anodes (readout channels)	2×256
Anode pitch	$294\ \mu\mathrm{m}$
Nominal operating voltage	-2.4 kV
Nominal bias of the collection region	-40 V
Nominal drift velocity	$8.1\ \mu\mathrm{m\ ns}^{-1}$
Nominal maximum drift time	$4.3\ \mu\mathrm{s}$
Cell size at nominal drift velocity	$294 \times 202\ \mu\mathrm{m}^2$
Cells per detector at nominal drift velocity	$2 \times 256 \times 174$
Total number of cells (260 SDDs)	$23 \times 16 \times 10^6$
Average resolution along the drift ($r\varphi$)	$35\ \mu\mathrm{m}$
Average resolution along the anode (z)	$25\ \mu\mathrm{m}$
Detection efficiency	99.5%
Average double-track resolution at 70% efficiency	$700\ \mu\mathrm{m}$

Silicon Strip Detectors (SSD)

The outer layers of the ITS are crucial for the connection of tracks from the TPC to the ITS. They also provide d*E/dx* information *to* assist particle identification for low-momentum particles. Both outer layers consist of double-sided Silicon Strip Detectors (SSD), mounted on carbon-fiber support structures identical to the ones which support the SDD. The detection module consists of one detector connected to two hybrids (see figure 3.14) featuring two layers of aluminum tracks. Each hybrid carries six frontend chips (HAL25). The system is optimized for low mass in order to minimize multiple scattering.

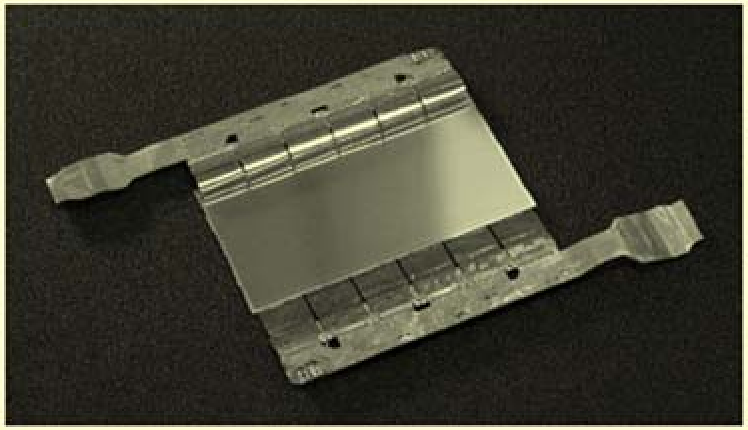

Number of HAL25 ASIC	20 376
Total number of channels	2 608 128
Number of DDL	16
Maximum hit rate per strip	50 Hz
Maximum L0 rate	75 kHz
Maximum L1 rate	6 kHz
Maximum L2 rate at 10% occupancy	1 kHz
Data volume/event at 10% occupancy	1 MB

Sensor active area	$73 \times 40\ mm^2$
Sensor total area	$75 \times 42\ mm^2$
Number of strips per sensor	2×768
Pitch of sensors on a ladder	39.1 mm
Strip pitch on a sensor	95 μm
Strip orientation p side	7.5 mrad
Strip orientation n side	27.5 mrad
Spatial precision $r\varphi$	20 μm
Spatial precision z	820 μm
Two track resolution $r\varphi$	300 μm
Two track resolution z	2400 μm
Radius layer 5 (lowest/highest)	378/384 mm
Radius layer 6 (lowest/highest)	428/434 mm
Number of ladders layer 5	34
Number of ladders layer 6	38
Modules per ladder layer 5	22
Modules per ladder layer 6	25
Number of modules layer 5	748
Number of modules layer 6	950
Material budget SSD cone	$0.28X_0$
Material budget per SSD layer	$0.81X_0$ (layer 5), $0.83X_0$ (layer 6)

Parameters of the various detector types. A module represents a single sensor element.

Parameter	Silicon pixel	Silicon drift	Silicon strip
Spatial precision $r\varphi$ (μm)	12	38	20
Spatial precision z (μm)	100	28	830
Two track resolution $r\varphi$ (μm)	100	200	300
Two track resolution z (μm)	850	600	2400
Cell size (μm^2)	50×425	150×300	$95 \times 40\,000$
Active area per module (mm^2)	12.8×69.6	72.5×75.3	73×40
Readout channels per module	40 960	2×256	2×768
Total number of modules	240	260	1698
Total number of readout channels (k)	9835	133	2608
Total number of cells (M)	9.84	23	2.6
Average occupancy (inner layer) (%)	2.1	2.5	4
Average occupancy (outer layer) (%)	0.6	1.0	3.3
Power dissipation in barrel (W)	1500	1060	1100
Power dissipation end-cap (W)	500	1750	1500

- 3-D reconstruction (< 100μm) of the Primary Vertex
- Secondary vertex Finding (Hyperons, D and B mesons)
- Particle identification via dE/dx for momenta < 1 GeV
- Tracking+Standalone reconstruction of very low momentum tracks

Time Projection Chamber (TPC)

The Time Projection Chamber (TPC) is the main particle tracking device in ALICE. Charged particles crossing the gas of the TPC (inner radius ~ 90 cm) knock electrons out of their atom, which then drift in the electric field. By measuring the arrival of electrons at the end of the chamber, the TPC will reconstruct the path of the original charged particles by reading out the energy they deposit in it.

Analyze individual event and perform charge hadron exclusive analysis. Two-track separation and momentum resolution.

Time Projection Chamber (TPC)

Pseudo-rapidity coverage	$-0.9 < \eta < 0.9$ for full radial track length
	$-1.5 < \eta < 1.5$ for 1/3 radial track length
Azimuthal coverage	2π
Radial position (active volume)	$845 < r < 2466$ mm
Radial size of vessel	$780 < r < 2780$ mm
Length (active volume)	5000 mm
Segmentation in φ	18 sectors
Segmentation in r	Two chambers per sector
Segmentation in z	Central membrane, readout on two end-plates
Total number of readout chambers	$2 \times 2 \times 18 = 72$
Inner readout chamber geometry	Trapezoidal, $848 < r < 1320$ mm active area
Pad size	4×7.5 mm ($\varphi \times r$)
Pad rows	63
Total pads	5504
Outer readout chamber geometry	Trapezoidal, $1346 < r < 2466$ mm active area
Pad size	6×10 and 6×15 mm ($\varphi \times r$)
Pad rows	$64+32 = 96$ (small and large pads)
Total pads	$4864+5120 = 9984$ (small and large pads)
Detector gas	Ne/CO_2 90/10
Gas volume	88 m^3
Drift length	2×2500 mm
Drift field	400 V cm^{-1}
Drift velocity	2.84 cm μs^{-1}
Maximum drift time	88 μs
Total HV	100 kV
Diffusion	$D_L = D_T = 220\ \mu m\ cm^{-1/2}$
Material budget	$X/X_0 = 3.5$ to 5% for $0 < \|\eta\| < 0.9$
Front-End Cards (FEC)	121 per sector $\times 36 = 4356$
Readout Control Unit (RCU) scheme	6 per sector, 18 to 25 FEC per RCU
Total RCUs	216
Total pads — readout channels	557 568
Pad occupancy (for $dN/dy = 8\,000$)	40–15% (inner/outer radius)
Pad occupancy (for pp)	$5\text{–}2 \times 10^{-4}$ (inner/outer radius)
Event size (for $dN/dy = 8000$)	~60 MB
Event size (for pp)	~1–2 MB depending on pile-up
Data rate limit	400 Hz Pb–Pb minimum bias events
Trigger rate limits	200 Hz Pb–Pb central events
	1000 Hz proton–proton events
ADC	10 bit
Sampling frequency	5.7–11.4 MHz
Time samples	500–1000
Conversion gain	6 ADC counts fC^{-1}
Position resolution (σ)	
In $r\varphi$	1100–800 μm (inner/outer radii)
In z	1250–1100 μm
dE/dx resolution	
Isolated tracks	5.5%
$dN/dy = 8000$	6.9%

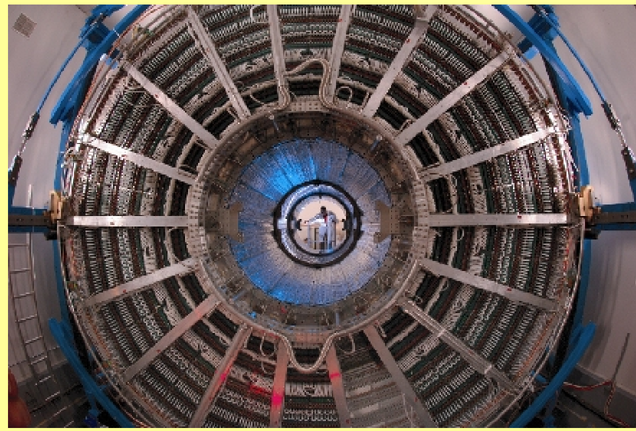

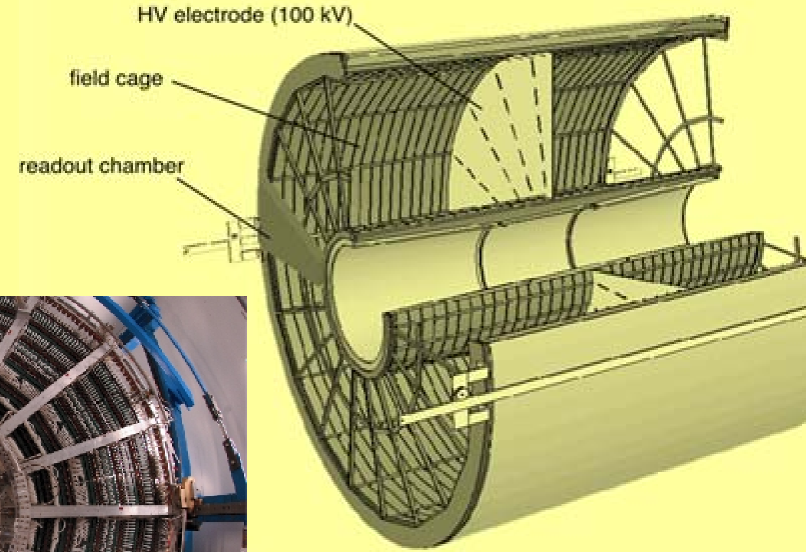

TPC schematic layout.

- Efficient (>90%) tracking in $\eta < 0.9$
- $\sigma(p)/p < 2.5\%$ up to 10 GeV/c
- Two-track resolution < 10 MeV/c
- PID with dE/dx resolution < 10%

Space-Point resolution 0.8 (1.2) mm in xy,(z), occupancy from 40% to 15%

Hadronic Observables with TPC

Both for AA, pA and pp collisions.

Hadronic measurements give information on the flavour composition of the particle-emitting source via the spectroscopy of strange and multi-strange hadrons (kaon, d meson, eta, phi etc.) via single- & two-particle spectra and correlations, and on event-by-event fluctuations.

Correlation observables place the highest demands on relative momentum and two-track resolution. For event-by-event analyses, large rapidity and pt acceptance are essential for the study of space–time fluctuations.

The detailed analysis of kaon spectra and the kaon-to-pion ratio on an event-by-event basis, more than 100 analysed kaons are required. Furthermore, event-plane reconstruction and flow studies require close to 2π azimuthal acceptance.

Heavy quarkonia, charmed and beauty particles, and high-pt jets, require very good momentum resolution at high momenta, which has to be achieved with the help of other tracking detectors. A large acceptance is also beneficial because of low production cross sections.

Specific Requirements on the TPC for Hadronic Observables

Momentum resolution: For soft hadronic observables momentum resolution on the level of 1% is required for momenta as low as 100 MeV/*c* *and for hard* probes set the requirements for the high-*pt region.* the momentum resolution for low-momentum tracks (between 100 MeV/*c* and 1 GeV/*c) reconstructed in the TPC is between 1 and 2%, depending on the magnetic* field setting. To measure higher momenta it is necessary to use the TPC in combination with the other tracking detectors (ITS and TRD). Using these detectors we can achieve about 10% momentum resolution for tracks with *pt of 100 GeV/c at 0.5 T magnetic field for* high-*pt region.*

Two-track resolution: Two-particle correlations efficiently resolution of about 5 MeV/c. For higher pt (about 1 GeV/c), the run at 0.5 T magnetic field.

d*E/dx resolution:* Particle identification by dE/dx measurement in the low-momentum (1/β2) region is achieved in certain momentum intervals, where the expected ionization for different particle types is well separated. For whole momentum range, up to a few GeV/c, need additional measurements (e.g. TOF detector). For even higher momenta, up to a few tens of GeV/c (relativistic rise region), at least on a statistical basis, to separate different hadron species if the dE/dx resolution is better than 7%. The resolution of the ionization measurements depends on the particle density, and a value of 6.9% is reached for the extreme multiplicities.

Specific Requirements on the TPC for Hadronic Observables

Track matching: Efficient track matching with the ITS detector is necessary to measure the track impact parameter at the interaction point and for secondary vertex reconstruction. In addition, matching with other tracking detectors will improve the momentum resolution significantly relative to stand-alone TPC reconstruction for tracks with momentum above a few GeV/c (e.g. an improvement by a factor 5 is expected for 10 GeV/c tracks). In order to increase the matching efficiency the thickness of the material between the detectors (i.e. the TPC field-cage and containment vessels) has to be kept to a minimum.

Azimuthal coverage: Full azimuthal coverage is necessary for global analysis of the event, such as the determination of the event plane, or flow analysis. Other signals, especially those limited by statistics, will benefit from a large azimuthal acceptance.

Leptonic Observables with TPC

Both for AA, pA and pp collisions.

The physics objectives of the ALICE central barrel have been extended with the addition of the Transition Radiation Detector (TRD). As a consequence, the performance and corresponding design criteria for the TPC, and for the other central barrel detectors, had to be reassessed and optimized taking into account the requirements for electron physics. In particular, the TPC design was optimized to provide the largest possible acceptance for full-length, high-pt tracks, in order to ensure significant statistics and good momentum resolution for high-mass and high-pt electron pairs. Therefore, the inactive areas between the readout chambers have been aligned towards the centre of the TPC. Electrons identified by the central barrel tracking detectors whose impact parameters are determined using the ITS will be used to measure charmed- and beauty-particle production. Moreover, impact-parameter measurement can be used to separate directly produced J/ψ mesons from those produced in B-decays.

Leptonic Observables with TPC

Tracking efficiency: The tracking efficiency for tracks with pt > 1 GeV/c that enter the TRD. The combined track finding in the central barrel detectors (ITS–TPC–TRD) has an efficiency well above 90% for these momenta.

Momentum resolution: The momentum resolution for electrons with transverse momentum around 5 GeV/c is better than 1.5% and keep the electron-pair mass resolution below 1% and thereby can resolve the members of the Υ family. This resolution is achieved using all the barrel tracking detectors (ITS–TPC–TRD) in combination at 0.5 T magnetic field.

dE/dx resolution: To achieve the required pion rejection factor (better than 200 at 90% electron identification efficiency) for momenta above 1 GeV/c, the TRD electron identification has to be complemented by the TPC dE/dx measurement, especially in the lower part of the momentum range, up to 3 GeV/c. In order to satisfy this requirement, the TPC must provide a dE/dx resolution better than 10% in the high-multiplicity environment of central Pb–Pb collisions. The expected precision for ionization measurement is significantly better than that required here. Simulation studies show that the electron identification capability is within the requirements of the present ALICE di-electron physics program.

Leptonic Observables with TPC

Rate capability: To inspect and track electron candidates identified in the TRD, the TPC should be operated at central collision rates of up to 200 Hz. Simulations have shown that, at this rate, the space charge due to the ion feed-back during gate-open time starts to be comparable to the space charge due to the ionization in the TPC drift volume itself.

Offline corrections for the space charge are expected to recover part of the resolution loss and should thus extend this limit. For pp runs with 5×10e30/cme2/s luminosity, the space charge due to both ionization in the drift volume and to the ion feed-back during gate-open time, is about one order of magnitude lower than for Pb–Pb, and thus not seen as a problem. Trigger rates of up to 1 kHz seem to be realistic.

High-Level Trigger (HLT): Given the discussed rate limitations, rare processes like J/ψ and ϒ production need a trigger to achieve useful statistics. The HLT is intended for this task. It is designed to find high-momentum electron tracks in the TRD and match them to the TPC tracks. The recorded data volume can be reduced using the ‘region-of-interest’ option of the trigger, reading out only the sectors of the TPC containing the data about the ‘interesting’, high-pt , tracks.

TRD

Forward detectors:

- Photon Mult. Det.
- Forward Multiplicity Detector, T0, V0, Zero Degrees Calorimeters

Specialized detectors:

- High Momentum PID
- PHOton Spectrometer

MUON Spectrometer

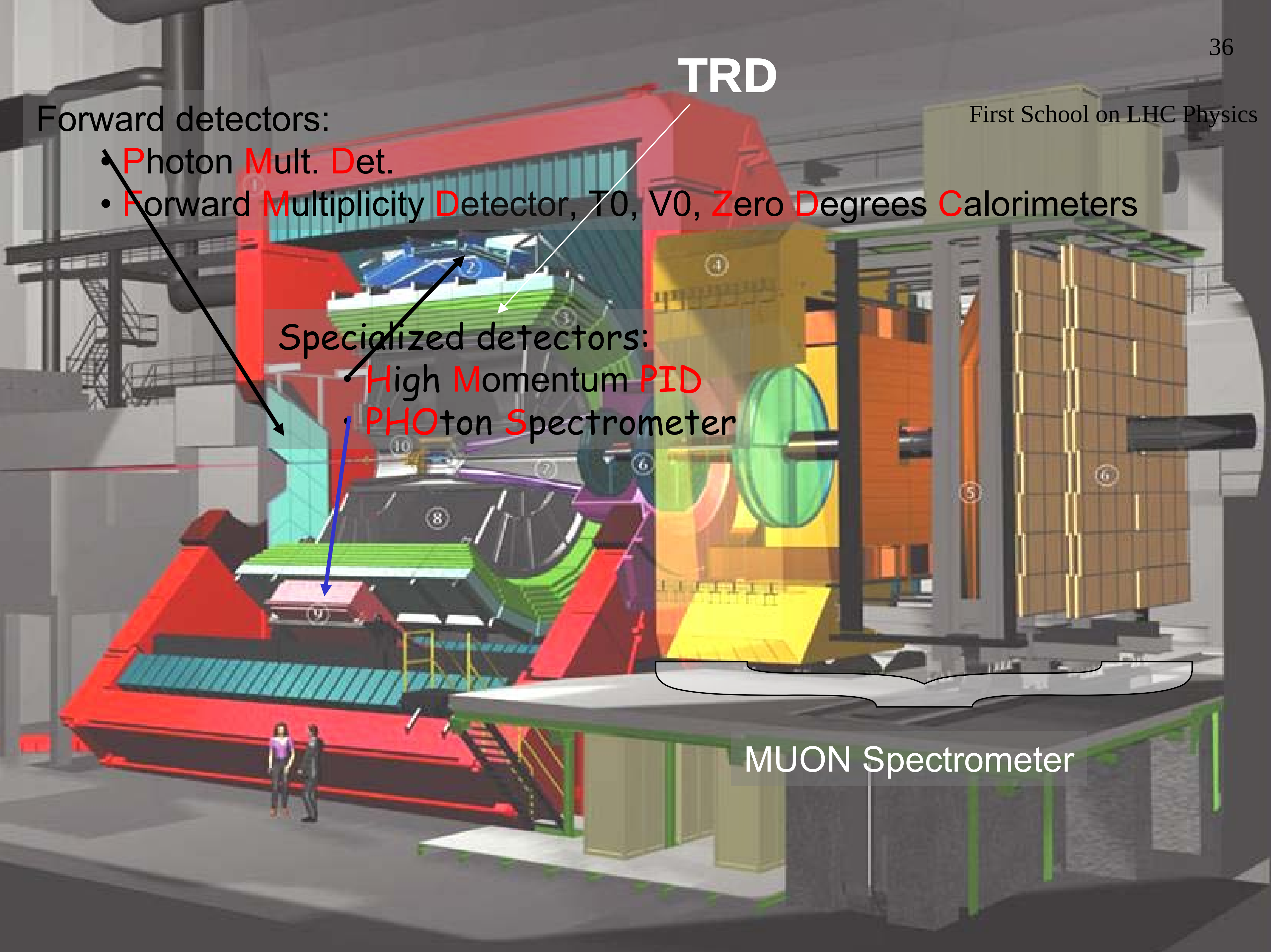

Transition Radiation Detector (TRD)

TRD is for electron identification in the central barrel for momenta greater than 1 GeV/c. As a consequence, the addition of the TRD significantly expands the ALICE physics objectives.

The TRD will provide, along with data from the TPC and ITS, sufficient electron identification to measure the production of light and heavy vector-meson resonances and the dilepton continuum in Pb–Pb and pp collisions.

In addition, the electron identification provided by the TPC and TRD for pt > 1 GeV/c can be used, in conjunction with the impact-parameter determination of electron tracks in the ITS, to measure open charm and open beauty produced in the collisions. A similar technique can be used to separate directly produced J/ψ mesons from those produced in B-decays.

These secondary J/ψ's could potentially mask the expected J/ψ yield modification due to quark–gluon plasma formation; their isolation is, therefore, of crucial importance for such measurements. Furthermore, since the TRD is a fast tracker, it can be used as an efficient trigger for high transverse momentum electrons. Such a trigger would considerably enhance the recorded ϒ yields in the high-mass part of the dilepton continuum as well as high-pt J/ψ.

Transition Radiation Detector (TRD)

Design Considerations:

- The required pion rejection capability is driven mostly by the J/ψ measurement and its pt dependence. the goal is an increase in pion rejection by a factor of 100 for electron momenta above 3 GeV/c. While the requirement for the ϒ is less stringent, the light vector mesons ρ, ω, and φ as well as the dielectron continuum between the J/ψ and the ϒ are only accessible with this level of rejection.

The required momentum resolution is determined by the matching to the TPC. The mass resolution of 100 MeV/c^2 at the ϒ for B = 0.4 T. The function that the TRD needs to fulfill is to add electron identification. This can be done by having pointing capability from the TRD to the TPC with an accuracy of a fraction of a TPC pad.

The thickness of the TRD in radiation lengths must be minimized since material generates additional background, mainly from photon conversion, and increases the pixel occupancy. Also, electron energy loss due to Bremsstrahlung removes electrons from the resonance reconstruction sample.

- The granularity of the TRD is driven in the bend direction by the required momentum resolution and along the beam direction by the required capability to identify and track electrons efficiently at the highest possible multiplicity. The detector has been designed for 80% single-track efficiency. The pads have an area of about 6 cm2 to attain the desired efficiency.
- Occupancy: As dNch/dη = 8000, the readout-pixel occupancy in central collisions

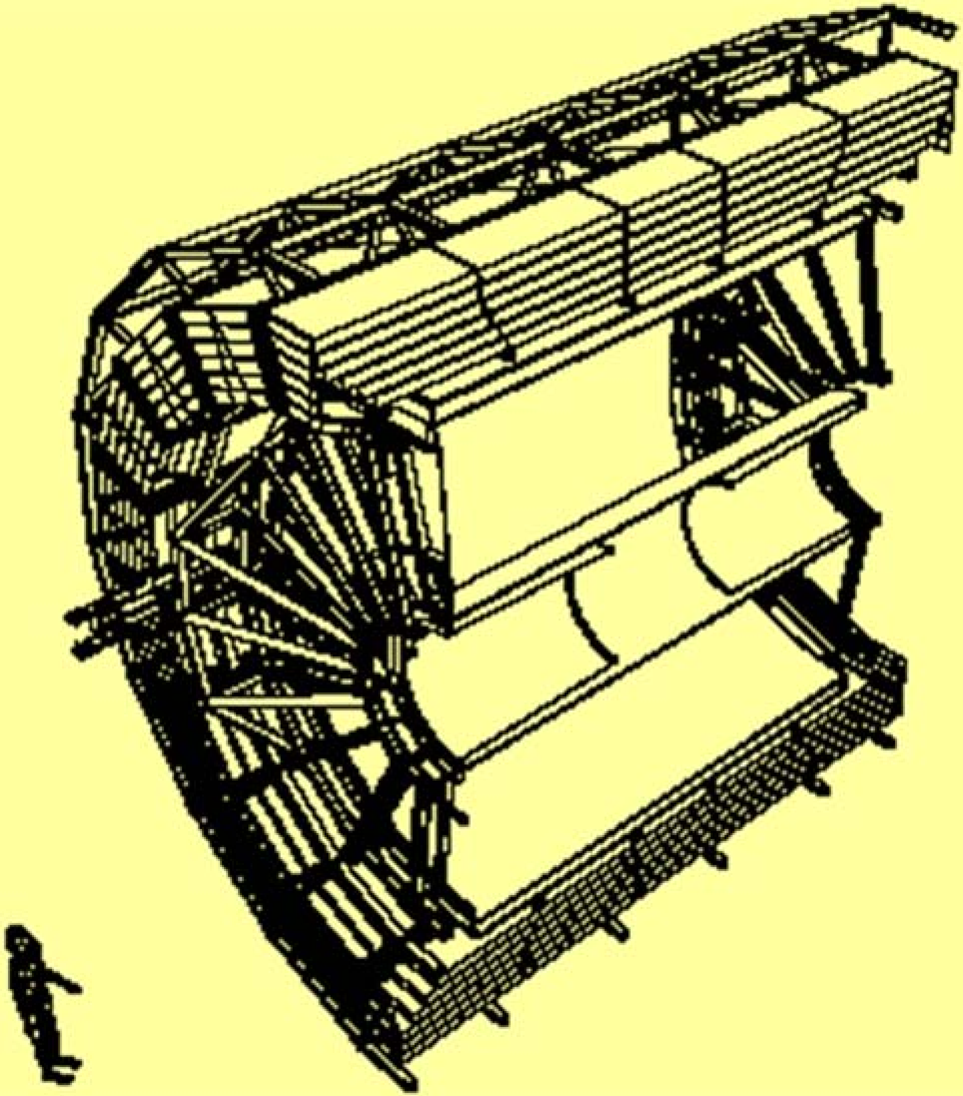

Cut through the ALICE TRD with the TPC inside.

Pseudo-rapidity coverage	$-0.9 < \eta < 0.9$
Azimuthal coverage	2π
Radial position	$2.9 < r < 3.7$ m
Length	Up to 7.0 m
Azimuthal segmentation	18-fold
Radial segmentation	Six layers
Longitudinal segmentation	5-fold
Total number of modules	540
Largest module	117×147 cm^2
Active detector area	736 m^2
Radiator	Fibres/foam sandwich, 4.8 cm per layer
Radial detector thickness	$X/X_0 = 15\%$
Module segmentation in φ	144
Module segmentation in z	12–16
Typical pad size	0.7×8.8 cm^{-2} = 6.2 cm^2
Number of pads	1.16×10^6
Detector gas	Xe/CO_2 (85%/15%)
Gas volume	27.2 m^3
Depth of drift region	3 cm
Depth of amplification region	0.7 cm
Nominal magnetic field	0.4 T
Drift field	0.7 kV cm^{-1}
Drift velocity	1.5 cm μs^{-1}
Longitudinal diffusion	$D_L = 250$ μm cm$^{-1/2}$
Transverse diffusion	$D_T = 180$ μm cm$^{-1/2}$
Lorentz angle	8°
Number of readout channels	1.16×10^6
Time samples in r (drift)	20
Number of readout pixels	2.32×10^7
ADC	10 bit, 10 MHz
Number of multi-chip modules	71 928
Number of readout boards	4108
Pad occupancy for $dN_{ch}/d\eta = 8000$	34%
Pad occupancy in pp	2×10^{-4}
Space-point resolution at 1 GeV c^{-1}	
in $r\varphi$	400 (600) μm for $dN_{ch}/d\eta = 2000$ ($dN_{ch}/d\eta = 8000$)
in z	2 mm (offline)
Momentum resolution	$\delta p/p = 2.5\% \oplus 0.5\%$ $(0.8\%)p$ for $dN_{ch}/d\eta = 2000$ ($dN_{ch}/d\eta = 8000$)
Pion suppression at 90% electron efficiency and $p \geqslant 3$ GeV c^{-1}	Better than 100
Event size for $dN_{ch}/d\eta = 8000$	11 MB (cf text)
Event size for pp	6 kB
Trigger rate limits for minimum-bias events	100 kHz
Trigger rate limits for pp	100 kHz (cf text)

High Momentum Particle Identification Detector (HMPID)

This measures fast moving particles by measuring their velocities.

HMPID, is dedicated to inclusive measurements of identified hadrons for pt > 1 GeV/c, is designed as a single-arm array with an acceptance of 5% of the central barrel phase space. The geometry of the detector was optimized with respect to particle yields at high-pt in both pp and AA collisions, and with respect to the large opening angle (corresponding to small effective size particle emitting sources) required for two-particle correlation measurements. Provide identification of particles beyond the momentum interval attainable through energy loss (in ITS and TPC) and time-of-flight measurements (in TOF).

The detector was optimized to extend the useful range for π/K and K/p discrimination, on a track-by-track basis, up to 3 and 5 GeV/c respectively.

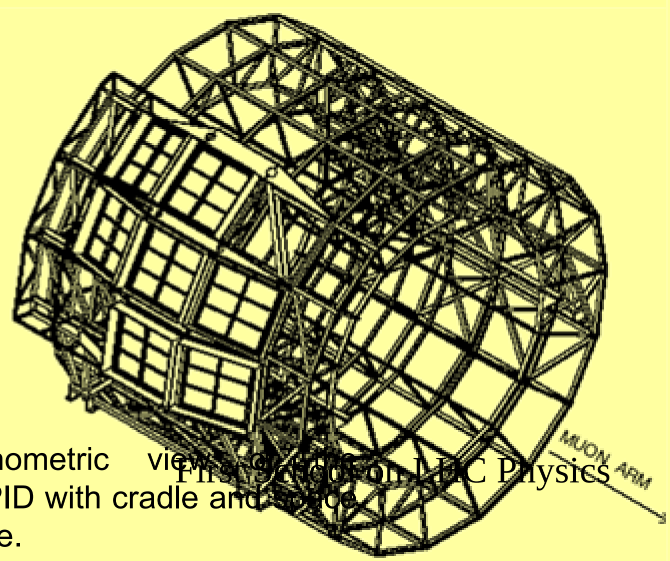

Axonometric view of the HMPID with cradle and space frame.

Pseudo-rapidity coverage	$-0.6 < \eta < 0.6$
Azimuthal coverage (rad)	57.61°
Radial position	5 m
Segmentation in φ	3-fold
Segmentation in z	3-fold
Total number of modules	7
Detector active area	10 m^2
Detector thickness radially	$X/X_0 = 18\%$
Radiator thickness	15 mm
Radiator medium	Liquid C_6F_{14}
Refractive index	1.2989 at 175 nm
Independent radiator trays	3 per module (21 total)
β threshold	0.77
Detector gas	CH_4
Gas volume	1.4 m^3
MWPC anode–cathode gap	2 mm
Operating voltage	2050 V
Photon converter	Cesium Iodide (CsI)
CsI thickness	300 nm
Quantum Efficiency (QE)	> 25% at 175 nm
Number of Photo-Cathodes (PC)	42
Number of pads per PC	3840 (161 280 total)
Pad size	8.0×8.4 mm^2 = 67.2 mm^2
Front-end chip (GASSIPLEX-07-3)	10 080
Peaking time	1.2 μs
Readout chip (DILOGIC-3)	3360
Front-end cards	3360
Readout cards	672
ADC (12-bit)	3360
Power consumption per module	500 W (total 3.5 kW)
Number of DDL	14
Multiplexing frequency	10 MHz (maximum)
Multiplexing time	5 μs at 10 MHz
Readout time (for 12% occupancy)	< 300 μs
Event size (for 12% occupancy)	< 0.1 MB
Number of readout channels	161 280
Occupancy ($dN_{ch}/d\eta = 8000$)	12%

Time Of Flight (TOF)

Design considerations. TOF detector of is a large area array that covers the central pseudo-rapidity region (|η| 0.9) for Particle Identification in the intermediate Momentum range (from 0.2 to 2.5 GeV/c). Since the majority of the produced charged particles is emitted in this range, the performance of such a detector is of crucial importance for the experiment. The measurement and identification of charged
particles in the intermediate momentum range will provide observables which can be used to probe the nature and dynamical evolution of the system produced in ultra-relativistic heavy-ion collisions at LHC energies.

The TOF, coupled with the ITS and TPC for track and vertex reconstruction and for dE/dx measurements in the momentum range up to ~ 0.5 GeV/c, provides event-byevent identification of large samples of pions, kaons, and protons. The TOF-identified particles will be used to study relevant hadronic observables on a single-event basis. In addition, at the inclusive level, identified kaons will allow invariant mass studies, in particular the detection of open charm states and the φ meson.

A large-coverage, powerful TOF detector, operating efficiently in extreme multiplicity conditions, should have an excellent intrinsic response and an overall occupancy not exceeding the 10–15% level at the highest expected charged-particle density (dNch/dη = 8000). This implies a design with more than 105 independent TOF channels. Since a large area has to be covered, a gaseous detector is the only choice. In the framework of the LAA project at CERN an intensive R&D program has shown that the best solution for the TOF detector is the Multi-gap Resistive-Plate Chamber (MRPC).

Time Of Flight (TOF)

The key aspect of these chambers is that the electric field is high and uniform over the whole sensitive gaseous volume of the detector. Any ionization produced by a traversing charged particle will immediately start a gas avalanche process which will eventually generate the observed signals on the pick-up electrodes. There is no drift time associated with the movement of the electrons to a region of high electric field. Thus the time jitter of these devices is caused by the fluctuations in the growth of the avalanche.

Advantages of MRPC technology w.r.t. other parallel-plate chamber designs:
- it operates at atmospheric pressure;
- the signal is the analogue sum of signals from many gaps, so there is no late tail and the charge spectrum is not of an exponential shape—it has a peak well separated from zero;
- the resistive plates quench the streamers so there are no sparks, thus high-gain operation becomes possible;
- the construction technique is in general rather simple and makes use of commercially available materials.

The latest tests of several MRPC multicell strip prototypes built with a double-stack structure show that these devices can reach an intrinsic time resolution better than about 40 ps and an efficiency close to 100%.

Time Of Flight (TOF)

Detect heavy particles by calculating the time they take to cover the distance of 3.7 m which separate the collision point from its barrel.

Large array at R ~ 3.7 m, covering | η| < 0.9 and full ϕ

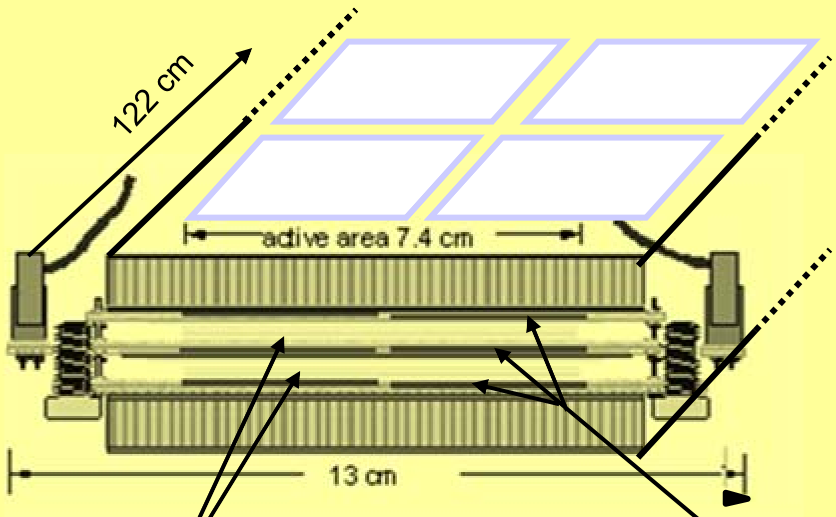

2x5 gas gaps of 250mm

Readout pads 3.5x2.5 cm^2

- TOF basic element: double-stack **Multigap RPC** strip
- Occupancy < 15% (**O**(10^5) readout channels)

Extensive R&D, from TB data:

- Intrinsic Resolution ~ 40 ps
- Efficiency > 99%

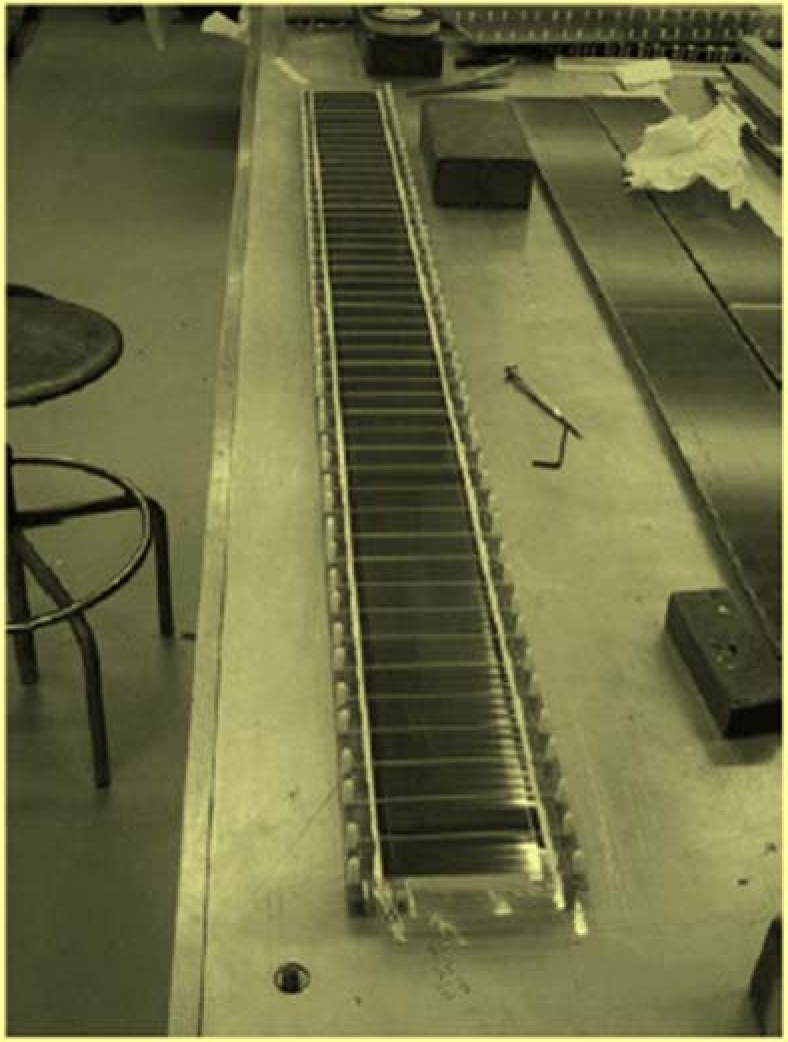

Photograph of an MRPC strip during construction.

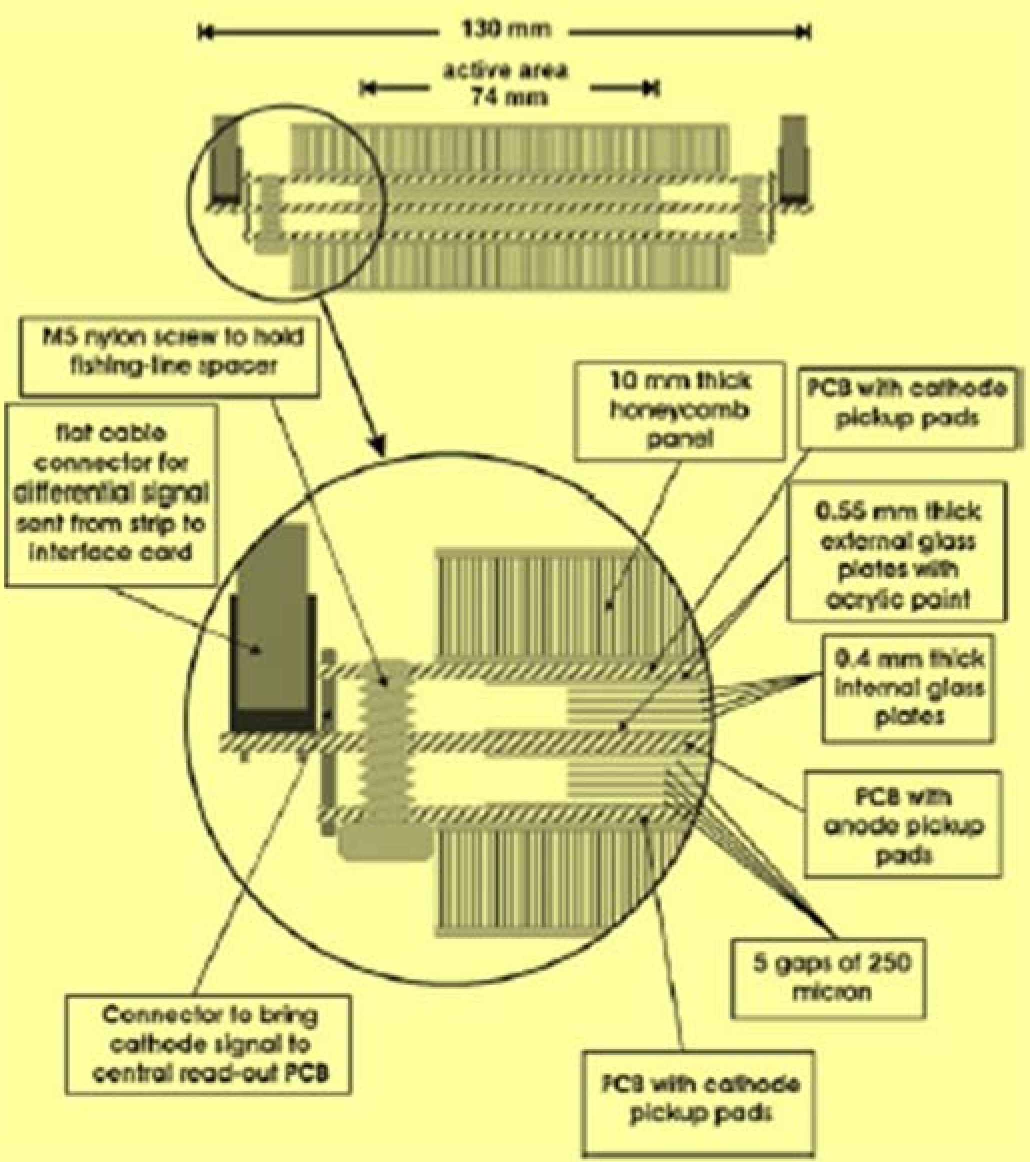

Cross section of a 10-gap double-stack MRPC strip.

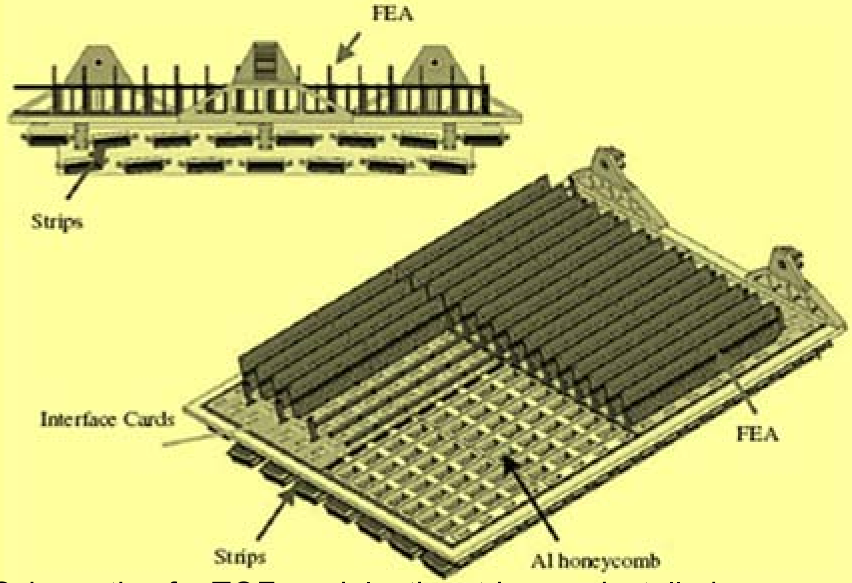

Schematic of a TOF module; the strips are installed inside the gas volume and the FEA cards are plugged onto the interface card. .

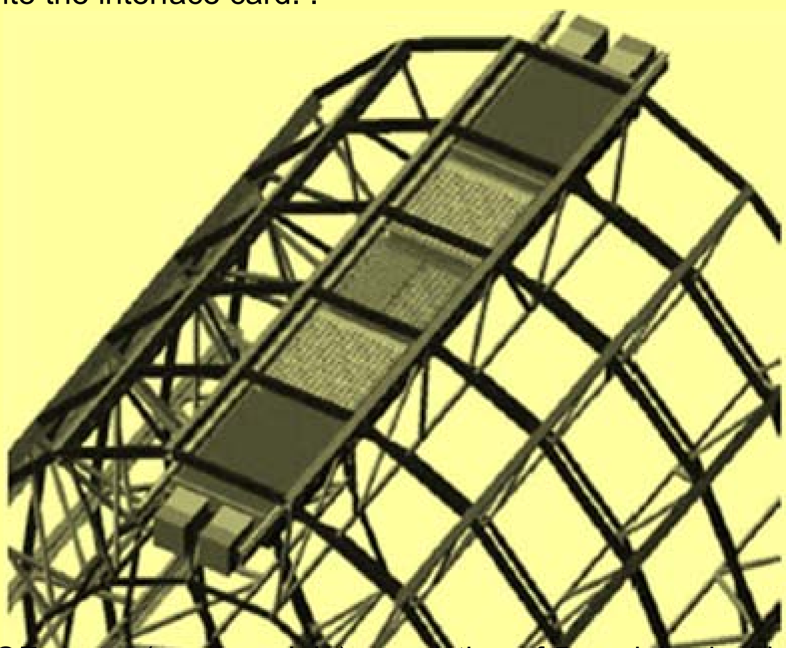
TOF sector (supermodule), consisting of 5 modules inside the space frame.

Synopsis of HMPID parameters.

Pseudo-rapidity coverage	$-0.9 < \eta < 0.9$
Azimuthal coverage	2π
Radial position	$3.70 < r < 3.99$ m
Length	7.45 m
Segmentation in φ	18-fold
Segmentation in z	5-fold
Total number of modules	90
Central module (A)	$117 \times 128\ \mathrm{cm}^2$
Intermediate module (B)	$157 \times 128\ \mathrm{cm}^2$
External module (C)	$177 \times 128\ \mathrm{cm}^2$
Detector active area	$141\ \mathrm{m}^2$
Detector thickness radially	$X/X_0 = 20\%$
Number of MRPC strips per module	15 (A), 19 (B), 19 (C)
Number of readout pads per MRPC strip	96
Module segmentation in φ	48 pads
Module segmentation in z	30 (A), 38 (B), 38 (C) pads
Readout pad geometry	$3.5 \times 2.5\ \mathrm{cm}^2$
Total number of MRPC strips	1638
Total number of readout pads	157 248
Detector gas	$C_2H_2F_4(90\%), i\text{-}C_4F_{10}(5\%), SF_6(5\%)$
Gas volume	$16\ \mathrm{m}^3$
Total flow rate	$2.7\ \mathrm{m}^3\ \mathrm{h}^{-1}$
Working pressure	<3 mbar
Fresh gas flow rate	$0.027\ \mathrm{m}^3\ \mathrm{h}^{-1}$
Number of readout channels	157 248
Number of front-end analogue chips (8-ch)	19 656
Number of front-end boards	6552
Number of HPTDC chips (8-ch, 24.4 ps bin width)	19 656
Number of HPTDC readout boards (TRM)	684
Number of readout boards (DRM) and crates	72
Occupancy for $dN_{ch}/d\eta = 8000$	13% ($B = 0.4$ T), 16% ($B = 0.2$ T)
Occupancy for pp	6×10^{-4}
π, K identification (with contamination $<10\%$)	0.2–2.5 GeV c^{-1}
p identification (with contamination $<10\%$)	0.4–4.5 GeV c^{-1}
e identification in pp (with contamination $<10\%$)	0.1–0.5 GeV c^{-1}
Event size for $dN_{ch}/d\eta = 8000$	100 kB
Event size for pp	<1 kB

PHOton Spectrometer (PHOS)

PHOS is a high-resolution spectrometer for detection of electromagnetic particles at central rapidity and provide photon identification as well as neutral mesons identification through the two-photon decay channel.

Physics objectives of PHOS:

Testing thermal and dynamical properties of the initial phase of the collision, in particular the initial temperature and space–time dimensions of the hot zone, through measurement of direct single-photon and diphoton spectra and direct photons.

Investigating jet quenching as a probe of deconfinement, through measurement of high-p_t π0 spectrum, and identifying jets through γ–jet and jet–jet correlations measurements.

The principal requirements on PHOS include the ability to identify photons, discriminate direct photons from decay photons and perform momentum measurements over a wide dynamic range with high energy and spatial resolutions.

Synopsis of PHOS parameters.

Coverage in pseudo-rapidity	$-0.12 \leqslant \eta \leqslant 0.12$
Coverage in azimuthal angle	$\Delta\varphi = 100°$
Distance to interaction point	4600 mm
Modularity	Five modules of 3584 crystals
EMCA	
Material	Lead-tungstate crystals (PWO)
Crystal dimensions	$22 \times 22 \times 180\,\mathrm{mm}^3$
Depth in radiation length:	20
Number of crystals	17 920
Segmentation	3584 crystals per module
Total area	$8\,\mathrm{m}^2$
Crystal volume	$1.5\,\mathrm{m}^3$
Total crystal weight	12.5 t
Operating temperature	−25 °C
CPV	
Gas	80% Ar/20% CO_2
Thickness	$0.5X_0$
Active area	$1.8\,\mathrm{m}^2 \times 14$ mm per module
Wire diameter:	30 μm
Number of wires per module	256
Wire pitch	5.65 mm
Pad size	$22 \times 10.5\,\mathrm{mm}^2$
Pad inter-distance	0.6 mm
Number of pads per module	7168

PHOton Spectrometer (PHOS)

Photon identification: Identified and discriminated against charged hadrons with a high efficiency, is achieved by applying criteria. (i) A high granularity segmentation so that showers induced by impinging particles develop over many adjacent cells. Topology analysis of the shower will be used to discriminate electromagnetic and hadronic showers. (ii) The measurement of the time of flight with resolutions of a few ns will provide means to discriminate photons and baryons (specially useful for neutron and antineutron discrimination). (iii) The addition of a charged-particle detector will enable to veto impacts from charged particles (electrons and charge hadrons). The topology analysis will also help to discriminate high-momentum photons and high-momentum $\pi 0$'s which decay into photons emitted in a cone too small to generate two distinct showers in PHOS.

High-energy resolution: The high-energy resolution needed to achieve $\pi 0$ identification through invariant mass analysis of the decay photons is achieved by using scintillator material of adequate thickness and which provide high photon–electrons yield. The light output must be readout by low-noise photodetectors and processed by low-noise front-end electronics.

High spatial resolution: The spatial resolution used for the particle induced shower spreads over several cells, allowing precise reconstruction of the impact point by calculating the centre of gravity of the shower.

Large dynamical range: Large dynamic range is achieved by selecting appropriate detector thickness to minimize shower leakage for the highest particle-energies without deterioration of energy resolution for lowest particle-energies due to light attenuation along the detector thickness. Using low-noise and high-gain photodetectors based on avalanche photo-diodes, which are insensitive to shower particles leaking out of the material, is required.

Electromagnetic Calorimeters of PHOS

Each EMCA module is segmented into 3584 detection channels arranged in 56 rows of 64 channels. The detection channel consists of a 22×22×180mm^3 lead-tungstate crystal, $PbWO_4$, coupled to a 5×5mm^2 APD which signal is processed by a low-noise preamplifier. The total number of crystals in PHOS is 17920 representing a total volume of □1.5m^3. The main mechanical assembly units in a module is the crystal strip unit consisting of eight crystal detector units forming 1/8 of a row. The APD and the preamplifier are integrated in a common body glued onto the end face of the crystal with optically transparent glue of a high refractive index.

To significantly (by about a factor of 3) increase the light yield of the $PbWO_4$ crystals (temperature coefficient □−2% per ◦C), the EMCA modules will be operated at a temperature of −25 ◦C. The temperature will be stabilized with a precision of □0.3 ◦C. To this purpose, the EMCA module is subdivided by thermo-insulation into a 'cold' and 'warm' volume. The crystal strips will be located in the 'cold' volume, whereas the readout electronics will be located outside this volume. All six sides of the 'cold' volume will be equipped with cooling panels, and heat is removed by a liquid coolant (hydrofluoroether) pumped through the channels of these panels. Temperature monitoring will be provided by means of a temperature measurement system, based on resistive temperature sensors of thickness 30–50 μm, which will be inserted in the gap between crystals.

A monitoring system using LED and stable current generators will monitor every EMCA detection channel. The system consists of Master Modules (MM) and Control Modules (CM). The MM (one per PHOS module) are located in the pit in the same VME crate as the PHOS trigger electronics. For each EMCA module there are 16 CM single channel 5–10 MeV Dynamic range 100 GeV Energy channels 'High' and 'low' gains Timing resolution Around 1 ns at 1–2 GeV Trigger L0, L1 Max channel counting rate in Pb–Pb 1 kHz in pp 10 Hz APD gain control Individual bias setting boards, located in the 'cold' volume of the EMCA modules, directly on top of the crystals. Each board, placed on a 15mm thick NOMEX plate, is equipped with a 16×14 LED matrix and the control and decoding circuits.

Forward Muon Spectrometer

Hard, penetrating probes, such as heavy-quarkonia states, are an essential tool for probing the early and hot stage of heavy-ion collisions. At LHC energies, energy densities high enough to melt the ϒ(1s) will be reached. Moreover, production mechanisms other than hard scattering might play a role. Since these additional mechanisms strongly depend on charm multiplicity, measurements of open charm and open beauty are of crucial importance (the latter also represents a potential normalization for bottomium). The complete spectrum of heavy quark vector mesons (i.e. J/ψ, ψ, ϒ, ϒ and ϒ), as well as the φ meson, will be measured in the $\mu^+\mu^-$ decay channel by the ALICE muon spectrometer. The simultaneous measurement of all the quarkonia species with the same apparatus will allow a direct comparison of their production rate as a function of different parameters such as transverse momentum and collision centrality. In addition to vector mesons, also the unlike-sign dimuon continuum up to masses around 10 GeV c^{-2} will be studied. Since at LHC energies the continuum is expected to be dominated by muons from the semi-leptonic decay of open charm and open beauty, it will also be possible to study the production of open (heavy) flavours with the muon spectrometer. Heavy-flavour production in the region $-2.5 < \eta < -1$ will be accessible through measurement of e–μ coincidences, where the muon is detected by the muon spectrometer and the electron by the TRD.

Forward Muon Spectrometer

The muon spectrometer participate in the general ALICE data taking for Pb–Pb collisions at L= 10^{27} $cm^{-2}s^{-1}$. The situation is different for intermediate-mass ion collisions (e.g. Ar–Ar) where the luminosity limitations from the machine are less severe. In this case, beside a general ALICE run at low luminosity L = 10^{27} $cm^{-2}s^{-1}$, to match the TPC rate capability, a high luminosity one L = 10^{29} $cm^{-2}s^{-1}$ is also foreseen, to improve the ϒ statistics. For the high-luminosity run, the muon spectrometer will take data together with a limited number of ALICE detectors (ZDC, ITS Pixel, PMD, T0, V0 and FMD) able to sustain the event rate.

Design criteria of the muon detector:

High multitrack capability: The tracking detectors of the spectrometer must be able to handle the high particle multiplicity.

Large acceptance: As the accuracy of dimuon measurements is statistics limited (ϒ family), the spectrometer geometrical acceptance must be as large as possible.

Low-pt acceptance: For direct J/ψ production it is necessary to have a large acceptance at low pt (at high pt a large fraction of J/ψ's is produced via b-decay).

Forward region: Muon identification in the heavy-ion environment is only feasible for muon momenta above □4 GeV/c because of the large amount of material (absorber) required to reduce the flux of hadrons. Hence, measurement of low-pt charmonia is possible only at small angles where muons are Lorentz boosted.

Muon Spectrometer

Summary of the main characteristics of the muon spectrometer.

Muon detection		
Polar, azimuthal angle coverage	$2° \leqslant \theta \leqslant 9°$, 2π	
Minimum muon momentum	$4\ \mathrm{GeV}\ c^{-1}$	
Resonance detection	J/ψ	Υ
Pseudo-rapidity coverage	$-4.0 \leqslant \eta \leqslant -2.5$	$-4.0 \leqslant \eta \leqslant -2.5$
Transverse momentum range	$0 \leqslant p_t$	$0 \leqslant p_t$
Mass resolution	70 MeV	100 MeV
Front absorber		
Longitudinal position (from IP)	$-5030\ \mathrm{mm} \leqslant z \leqslant -900\ \mathrm{mm}$	
Total thickness (materials)	$\sim 10\lambda$ (carbon–concrete–steel)	
Dipole magnet		
Nominal magnetic field, field integral	0.7 T, 3 T m	
Free gap between poles	2.972–3.956 m	
Overall magnet length	4.97 m	
Longitudinal position (from IP)	$-z = 9.87$ m (centre of the dipole yoke)	
Tracking chambers		
Number of stations, number of planes per station	5, 2	
Longitudinal position of stations	$-z = 5357, 6860, 9830, 12\,920, 14\,221$ mm	
Anode–cathode gap (equal to wire pitch)	2.1 mm for st. 1; 2.5 mm for st. 2–5	
Gas mixture	80% Ar/20% CO_2	
Pad size st. 1 (bending plane)	$4 \times 6, 4 \times 12, 4 \times 24\ \mathrm{mm}^2$	
Pad size st. 2 (bending plane)	$5 \times 7.5, 5 \times 15, 5 \times 30\ \mathrm{mm}^2$	
Pad size st. 3, 4 and 5 (bending plane)	$5 \times 25, 5 \times 50, 5 \times 100\ \mathrm{mm}^2$	
Max. hit density st. 1–5 (central Pb–Pb × 2)	$5.0, 2.1, 0.7, 0.5, 0.6 \cdot 10^{-2}$ hits cm^{-2}	
Spatial resolution (bending plane)	$\simeq 70\ \mu\mathrm{m}$	
Tracking electronics		
Total number of FEE channels	1.09×10^6	
Shaping amplifier peaking time	$1.2\ \mu\mathrm{s}$	
Trigger chambers		
Number of stations, number of planes per station	2, 2	
Longitudinal position of stations	$-z = 16\,120, 17\,120$ mm	
Total number of RPCs, total active surface	72, $\sim 150\ \mathrm{m}^2$	
Gas gap	single, 2 mm	
Electrode material and resistivity	Bakelite™, $\rho = 2\text{–}4 \times 10^9\ \Omega\,\mathrm{cm}$	
Gas mixture	Ar/$C_2H_2F_4$/i-butane/SF_6 ratio 49/40/7/1	
Pitch of readout strips (bending plane)	10.6, 21.2, 42.5 mm (for trigger st. 1)	
Max. strip occupancy bend. (non bend.) plane	3% (10%) in central Pb–Pb	
Maximum hit rate on RPCs	3 (40) Hz cm^{-2} in Pb–Pb (Ar–Ar)	
Trigger electronics		
Total number of FEE channels	2.1×10^4	
Number of local trigger cards	234 + 2	

Invariant-mass resolution: A resolution of dimuon invariant-mass region is needed to resolve the J/ψ and ψ (ϒ, ϒ and ϒ) peaks. This requirement determines the bending strength of the spectrometer magnet as well as the spatial resolution of the muon tracking system. It also imposes the minimization of multiple scattering and a careful optimization of the absorber.

Trigger: The spectrometer has to be equipped with a selective dimuon trigger system to match the maximum trigger rate of about 1 kHz handled by the DAQ.

At one side of the barrel, where it will detect muons emitted at small angles w.r.t the beam. Detect m and measure their momenta from the bending of their tracks in a magnetic field.

Zero Degree Calorimeters

The observable most directly related to the geometry of the collision is the number of participant nucleons, which can be estimated by measuring the energy carried in the forward direction (at zero degree relative to the beam direction) by non-interacting (spectator) nucleons. The zero degree forward energy decreases with increasing centrality. Spectator nucleons will be detected in ALICE by means of Zero-Degree Calorimeters (ZDC). In the ideal case, in which all spectators are detected, the estimate of the number of participants is deduced from the measurement as,

$E_{ZDC}(\mathrm{TeV}) = 2.76 N_{spectators}$, $N_{participants} = A - N_{spectators}$,

where 2.76 TeV is the nucleon energy of the Pb beam at LHC. Such a simple estimate can however not be used at a collider since not all the spectator nucleons can be detected.

Cross section of the beam line 115m from the interaction point.

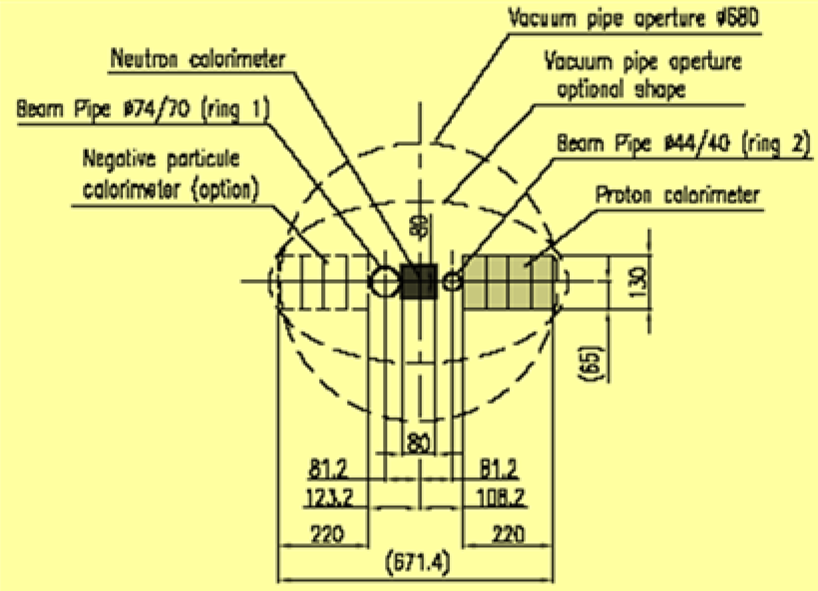

Dimensions and main characteristics of absorber and quartz fibers for neutron and proton calorimeters..

	ZN	ZP
Dimensions (cm^3)	$7.04 \times 7.04 \times 100$	$12 \times 22.4 \times 150$
Absorber	Tungsten alloy	Brass
$\rho_{absorber}$ (g cm^{-3})	17.61	8.48
Fibre core diameter (μm)	365	550
Fibre spacing (mm)	1.6	4
Filling ratio	1/22	1/65

Hadron Calorimeters of ZDC

The neutron ZDC has the most severe geometrical constraint and therefore the detector transverse dimension ~7 cm and a very dense passive material has been used to maximize containment of showers generated by neutrons of 2.76 TeV.

For the proton ZDC there are no such stringent space constraints and, moreover, spectator protons spot has a large spatial distribution.

A larger detector made of a less dense material can therefore be used. Another important characteristic for these detectors is the fiber spacing that should not be greater than the radiation length of the absorber to avoid electron absorption in the passive material.

The energy resolution of the ZDCs is a fundamental parameter in the design of the devices. The physics performance of the detector for the measurement of the centrality of the collision is in fact directly related to the resolution on the number of spectator nucleons which hit the calorimeters' front faces. Therefore a good energy resolution is a necessary prerequisite for a reliable estimation of the centrality variables.

	ZN	ZP
Dimensions (cm^3)	$7.04 \times 7.04 \times 100$	$12 \times 22.4 \times 150$
Absorber	Tungsten alloy	Brass
$\rho_{absorber}$ ($g\,cm^{-3}$)	17.61	8.48
Fibre core diameter (μm)	365	550
Fibre spacing (mm)	1.6	4
Filling ratio	1/22	1/65

Dimensions and main characteristics of absorber and quartz fibers for neutron and proton calorimeters..

Electromagnetic Calorimeters of ZDC

The EM ZDC project includes a forward electromagnetic calorimeter to improve the centrality trigger. It is designed to measure, event by event, the energy of particles emitted at forward rapidities, essentially photons generated from π^0 decays.

The detection technique employed for the electromagnetic calorimeter is the same as the one used for the hadronic calorimeters. The most important difference consists in the choice of the angle of the fibers relative to incoming particles. Fibers are oriented at 45°, while for the hadronic calorimeters they are at 0°. This choice maximizes the detector response, since Cherenkov light production has a pronounced peak around 45°. The electromagnetic calorimeter is made of lead, with quartz fibers sandwiched in layers between the absorber plates. Two consecutive planes of fibers are separated by a lead thickness of 3 mm which, due to the 45° inclination, results in a total thickness of 4.24mm seen by incident particles. Fiber cores have a diameter of 550 μm. The resulting calorimeter dimensions are 7×7×21 cm^3, the total absorber length corresponding to about 30 radiation lengths.

The ZDC location is at 116 m from the interaction point above the neutron calorimeter, just outside the cone of spectator neutrons. The pseudo-rapidity range covered by the two detectors, placed on both sides relative to interaction point , is between 7.8 and 9.2 m.

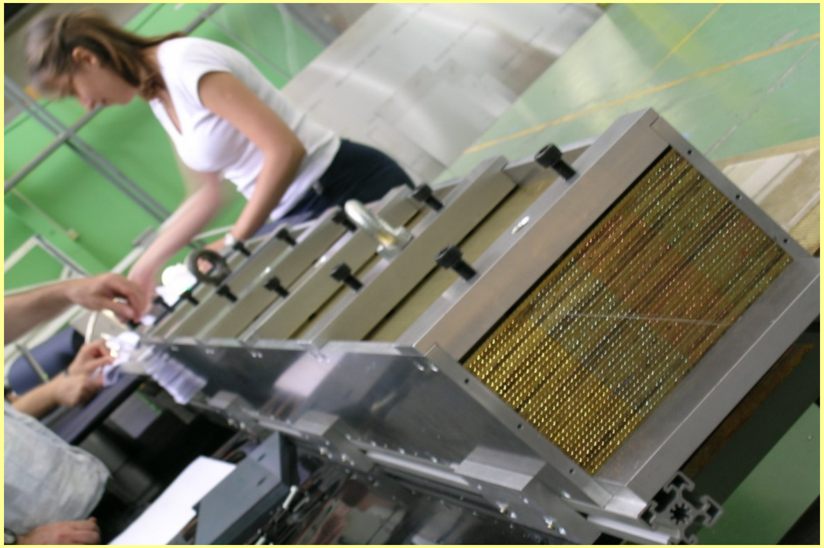

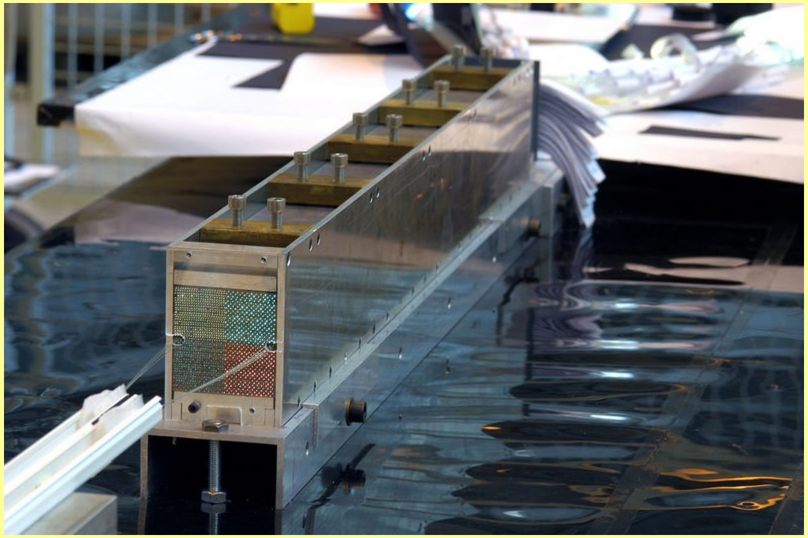

Photon Multiplicity Detector (PMD)

PMD is a pre-shower detector that measures the multiplicity and spatial (η–φ) distribution of photons on an event-by-event basis in the forward region of ALICE. The PMD addresses physics issues related to event-byevent fluctuations, and provides estimates of transverse electromagnetic energy and the reaction plane on an event-by-event basis .

The PMD consists of two identical planes of detectors with thick lead converter in between them. The front detector plane is used for vetoing charged-particle hits. The detector plane behind the converter is the preshower plane which registers hits from both photons and charged hadrons.

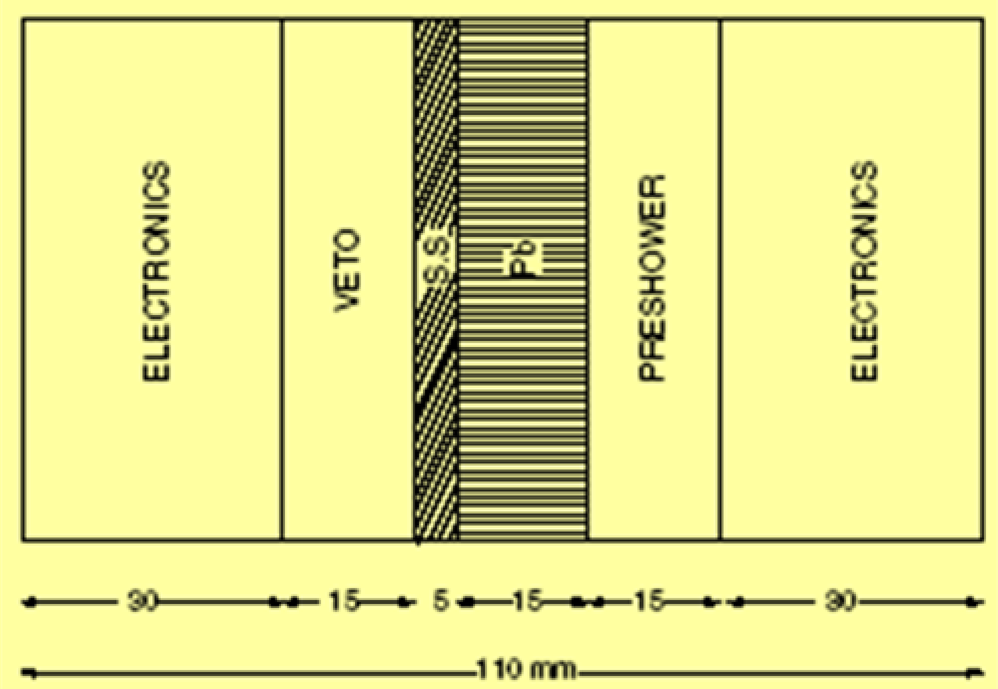

Cross section of the PMD (schematic only) showing the veto plane, lead converter and the preshower plane. SS is the support plate on which lead plates and the detectors will be mounted.

The PMD consists of two identical planes of detectors with thick lead converter in between them. The front detector plane is used for vetoing charged-particle hits. The detector plane behind the converter is the preshower plane which registers hits from both photons and charged hadrons.

Photon Multiplicity Detector (PMD)

Summary of design and operating parameters of the PMD.

Pseudorapidity coverage	$2.3 \leqslant \eta \leqslant 3.5$
Azimuthal coverage	2π
Distance from vertex	361.5 cm
Detector active area	2 m^2
Detector weight	1200 kg
Number of planes	two (Veto and Preshower)
Converter	$3X_0$ lead
Hexagonal cell cross section	0.22 cm^2
Hexagonal cell depth (gas thickness)	0.5 cm
Detector gas	Ar/CO_2 (70%/30%)
Operating voltage	−1400 V
Charged-particle detection efficiency	96%
Number of supermodules per plane	4
Number of unit modules per supermodule	6
Number of cells in a unit module	4608
Number of HV channels	48
Total number of cells	221 184
Number of FEE boards	3456
Number of CROCUS crates	4
Number of DDL channels	4
Cell occupancy for $dN_{ch}/d\eta = 8000$ for veto plane	13%
Cell occupancy for $dN_{ch}/d\eta = 8000$ for preshower plane	28%
Average photon reconstruction efficiency	54%
Average purity of photon sample	65%
Event size for $dN_{ch}/d\eta = 8000$	0.12 MB
Average time for readout of event	100 μs

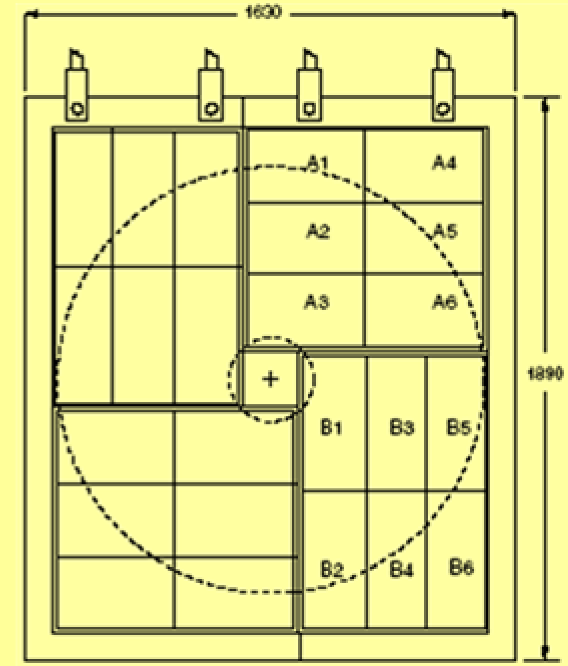

Layout of the PMD showing four supermodules. Each supermodule has six unit modules. The detector has full azimuthal coverage in the region 2.3<η<3.5. The inner hole is 22 cm×20 cm.

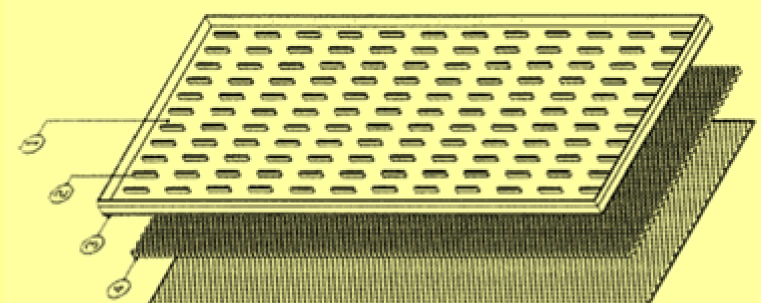

Components of a unit module: (1) top PCB, (2) 32-pin connector, (3) HV isolation and gas seal, (4) copper honeycomb, (5) bottom PCB showing islands of insulation circles.

Forward Multiplicity Detectors (FMD)

The main functionality of the silicon strip (# 5120) FMD is to provide charged-particle multiplicity information in the pseudo-rapidity range $-3.4 < \eta < -1.7$ and $1.7 < \eta < 5.1$, is for the study of multiplicity fluctuations on an event-by-event basis and for flow analysis (relying on the azimuthal segmentation). Together with the pixel system of the ITS, the FMD will provide early charged particle multiplicity distributions for all collision types in the range $-3.4 < \eta < 5.1$. Overlap between the various rings and with the ITS inner pixel layer provides redundancy and important checks of analysis procedures.

The average number of hits for very central Pb–Pb collision, assuming the extreme charged-particle multiplicity density of $dN_{ch}/d\eta \approx 8000$, and including background from secondary interactions, will be less than 3 charged particles per strip for all channels. The majority of channels will on average be traversed by about one charged particle per central event. For these, multiplicity information may be obtained by comparing the number of occupied and empty channels. In general, however, multiplicity information will be obtained by measuring the energy deposition in each channel and relating this to the number of charged particles and to provide information for the trigger system at the earliest possible moment

The distance z, from the detector to the IP, the inner and outer radii, and the resulting pseudo-rapidity coverage of each ring.

Ring	z (cm)	R_{in} (cm)	R_{out} (cm)	η coverage
Si1 outer	−75.2	15.4	28.4	$-2.29 < \eta < -1.70$
Si1 inner	−62.8	4.2	17.2	$-3.40 < \eta < -2.01$
Si2 outer	75.2	15.4	28.4	$1.70 < \eta < 2.29$
Si2 inner	83.4	4.2	17.2	$2.28 < \eta < 3.68$
Si3	340.0	4.2	17.2	$3.68 < \eta < 5.09$

Physical dimensions of Si segments and strips, together with the average number of charged particles hitting each strip in central Pb–Pb collisions.

	Radial coverage (cm)	Particle flux (cm^{-2})	Azimuthal sectors	Radial strips	Strip area (cm^2)	Average number of hits
Si1 inner	4.2–17.2	10–65	20	512	0.03–0.14	2.2–1.4
Si1 outer	15.4–28.4	3–8	40	256	0.12–0.23	1.0–0.7
Si2 inner	4.2–17.2	8–35	20	512	0.03–0.14	1.2–1.1
Si2 outer	15.4–28.4	3–8	40	256	0.12–0.23	1.0–0.7
Si3	4.2–17.2	6–27	20	512	0.03–0.14	0.9–0.8

Forward Multiplicity Detectors (FMD)

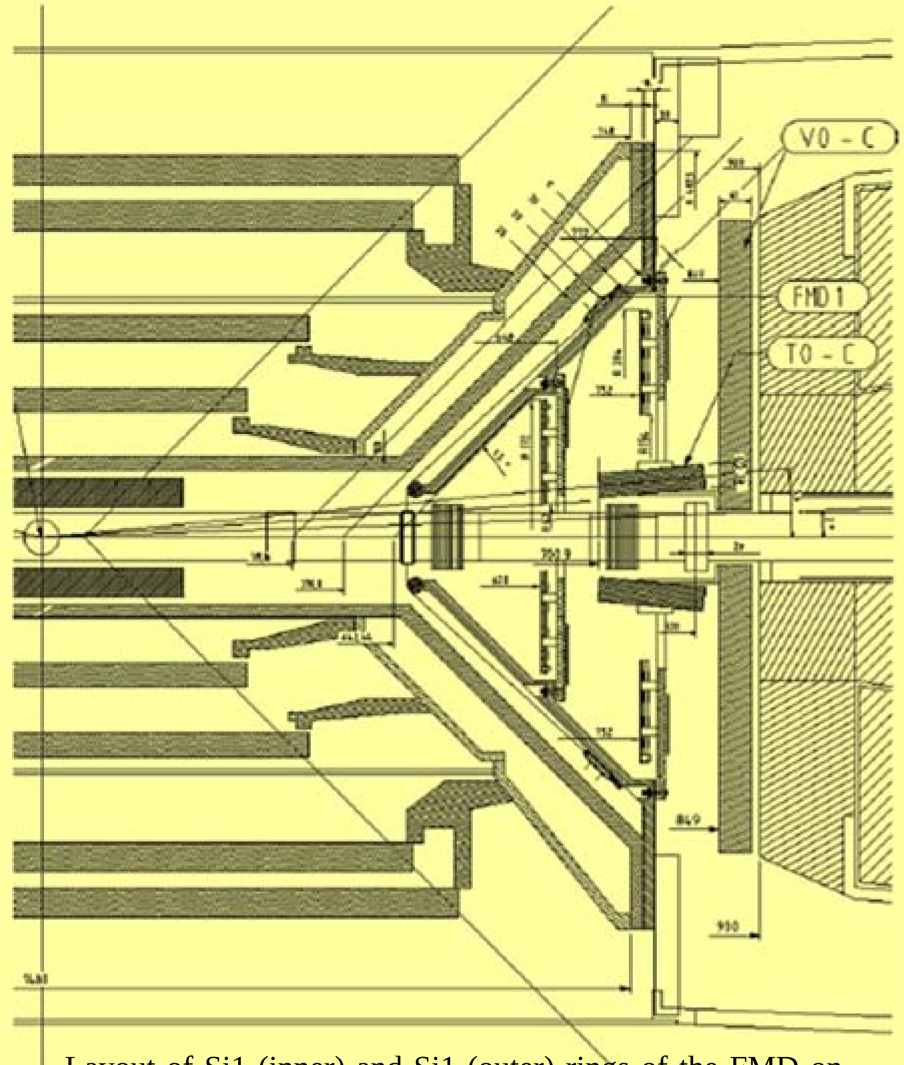

Layout of Si1 (inner) and Si1 (outer) rings of the FMD on the muon absorber side of the IP. The figure also shows the location of the T0 and V0 detectors.

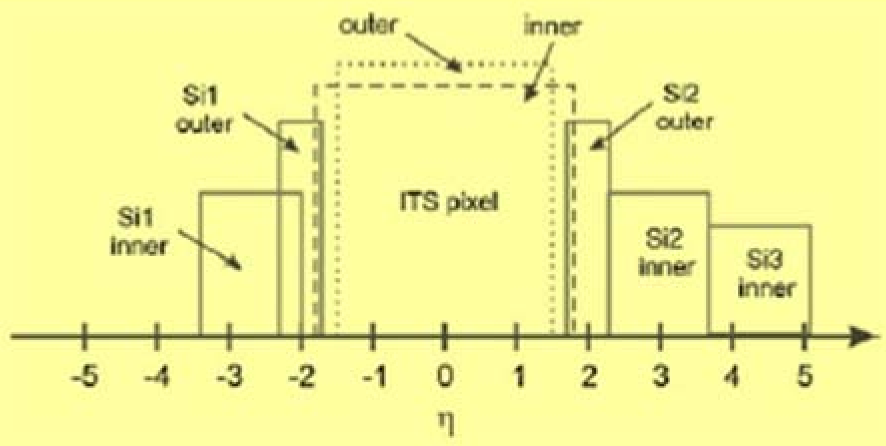

Physical dimensions of Si segments and strips, together with the average number of charged particles hitting each strip in central Pb–Pb collisions.

Forward Multiplicity Detectors (FMD)

Proposed assembly of an inner Si ring showing mechanical support plates and hybrid cards with each one Si sensor. The sensors will be glued to the hybrid cards and the strips wire bonded to the hybrids. The glued segments are attached to the support plate by screws on the feet. Shown on the hybrid cards are FE chips along the two radial edges, other electronic components and connectors for the cables. The support plates will also carry the FMD Digitizer boards on the back side.

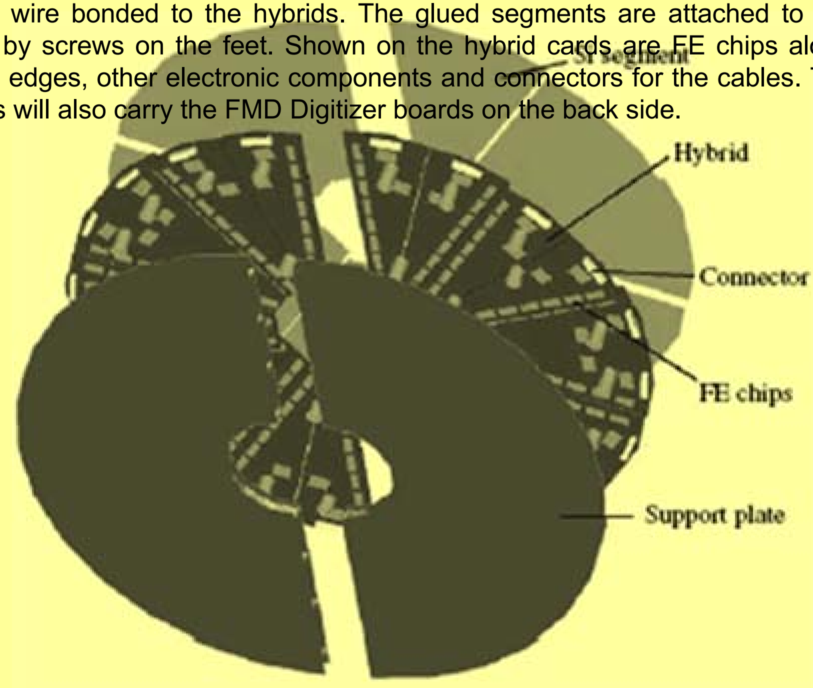

The total number of strip channels per ring and the number of front-end (FE) preamplifier chips (128 channels per chip are listed). Also shown is the number ofALTRO readout chips for each ring and the number of digitizer cards envisaged to carry these. One readout controller unit (RCU) is foreseen at each side of the IP.

	FE channels	FE chips	ALTRO chips	FMD digitizers	RCU modules
Si1 inner	10 240	80	6	2	1
Si1 outer	10 240	80	6	2	
Si2 inner	10 240	80	6	2	1
Si2 outer	10 240	80	6	2	
Si3	10 240	80	6	2	
Total system	51 200	400	30	10	2

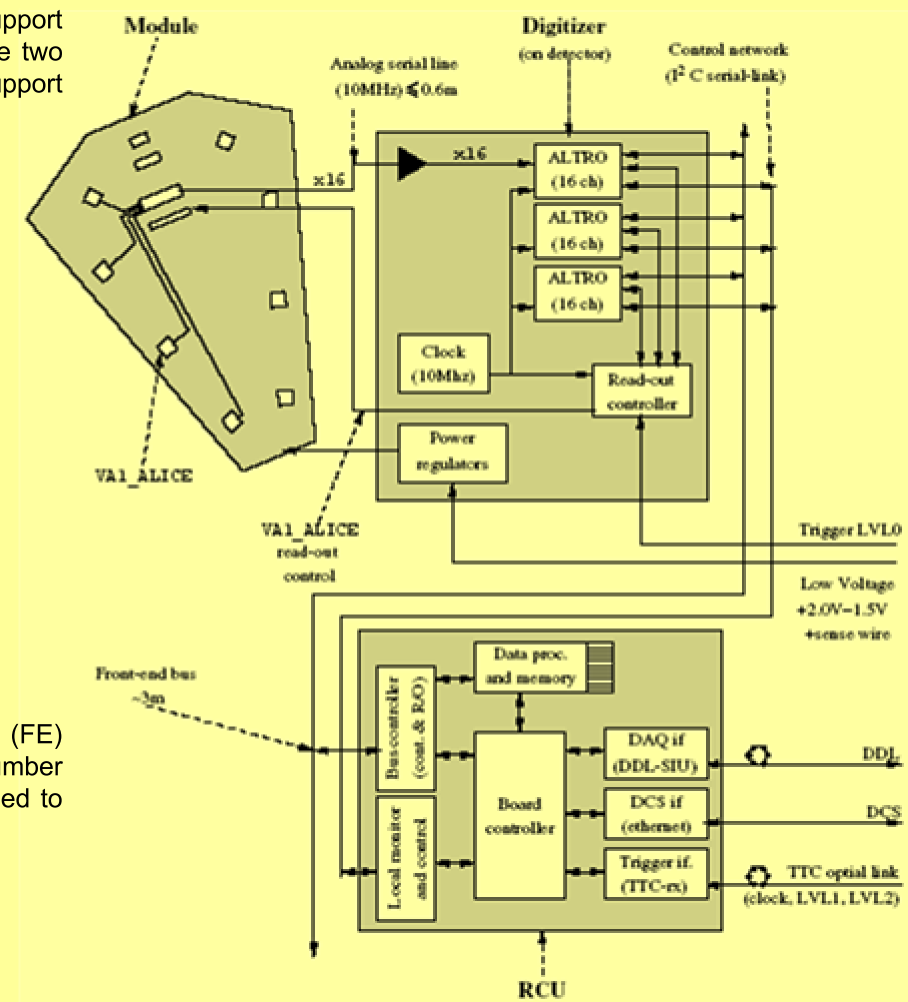

Schematics of the full electronics chain of the FMD detectors. A silicon detector segment with its hybrid is shown, followed by a FMD Digitizer card with one ADC channel per FE amplifier chip, the FMD Readout Controller Unit (FMD-RCU) and the DDL, DCS and Trigger links.

V0 Detectors

The V0 detector has multiple roles. It provides:

- a minimum bias trigger for the central barrel detectors;
- two centrality triggers in Pb–Pb collisions;
- a centrality indicator;
- a control of the luminosity;
- a validation signal for the muon trigger to filter background in pp mode.

Special care must be taken to minimize the background due to the location of the V0 detector. Indeed, the presence of important material volumes (beam pipe, front absorber, FMD, T0, ITS services) in front of the V0 arrays will generate an important number of secondaries (mainly electrons) which will affect physical information about the number of charged particles. The efficiency of minimum bias triggering and the multiplicity measurement will be strongly modified by this secondary particle production. Beam–gas interactions will be another source of background. It will provide triggers which have to be identified and eliminated. This background is particularly important in pp runs.
Measuring the time-of-flight difference between two detectors located on each side of the interaction point will enable to identify these background events. The V0 detector must therefore provide signal charge and time-of-flight measurement capabilities.

V0 Detectors

Segmentation of the V0A/V0C arrays.

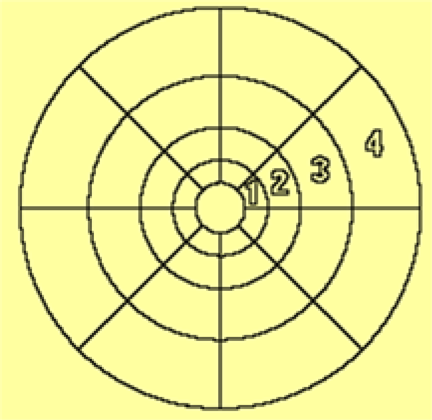

V0A and V0C arrays. Pseudo-rapidity coverage and angular acceptance (in deg) of the rings.

	V0A		V0C	
Ring	η_{max}/η_{min}	$\theta_{min}/\theta_{max}$	η_{max}/η_{min}	$(\pi-\theta)_{min}/(\pi-\theta)_{max}$
1	5.1/4.5	0.7/1.3	−3.7/−3.2	2.8/4.7
2	4.5/3.9	1.3/2.3	−3.2/−2.7	4.7/7.7
3	3.9/3.4	2.3/3.8	−2.7/−2.2	7.7/12.5
4	3.4/2.8	3.8/6.9	−2.2/−1.7	12.5/20.1

T0 Detectors

The T0 detectors have to perform the following functions:

1.To generate a T0 signal for the TOF detector. This timing signal corresponds to the real time of the collision (plus a fixed time delay) and is independent on the position of the vertex. The required precision of the T0 signal is about 50 ps (r.m.s.).

2.To measure the vertex position (with a precision±1.5 cm) for each interaction and to provide a L0 trigger when the position is within the preset values. This will discriminate against beam–gas interactions.

3.To provide an early 'wake-up' signal to TRD, prior to L0.

4.To measure the particle multiplicity and generate one of the three possible trigger signals:

$T0_{min-bias}$, $T0_{semi-central}$, or $T0_{central}$.

Since the T0 detector generates the earliest L0 trigger signals, they must be generated online without the possibility of any offline corrections. The dead time of the detector should be less than the bunch-crossing period in pp collisions (i.e. < 25 ns).

One of the arrays, labeled $T0_R$ ($2.9< \eta<3.3$) is placed 70 cm from the nominal vertex. Such a small distance had to be chosen because of the space constraints imposed by the front cone of the muon absorber and other forward detectors. On the opposite side the distance of the left array, T0L, is about 350 cm—comfortably far from the congested central region. T0L is grouped together with the other forward detectors (FMD, V0, and PMD) and covers the pseudo-rapidity range of $-5<\eta<-4.5$. In the radial (transverse) direction both T0 arrays are placed as close to the beam pipe as possible to maximize triggering efficiency.

T0 Detectors

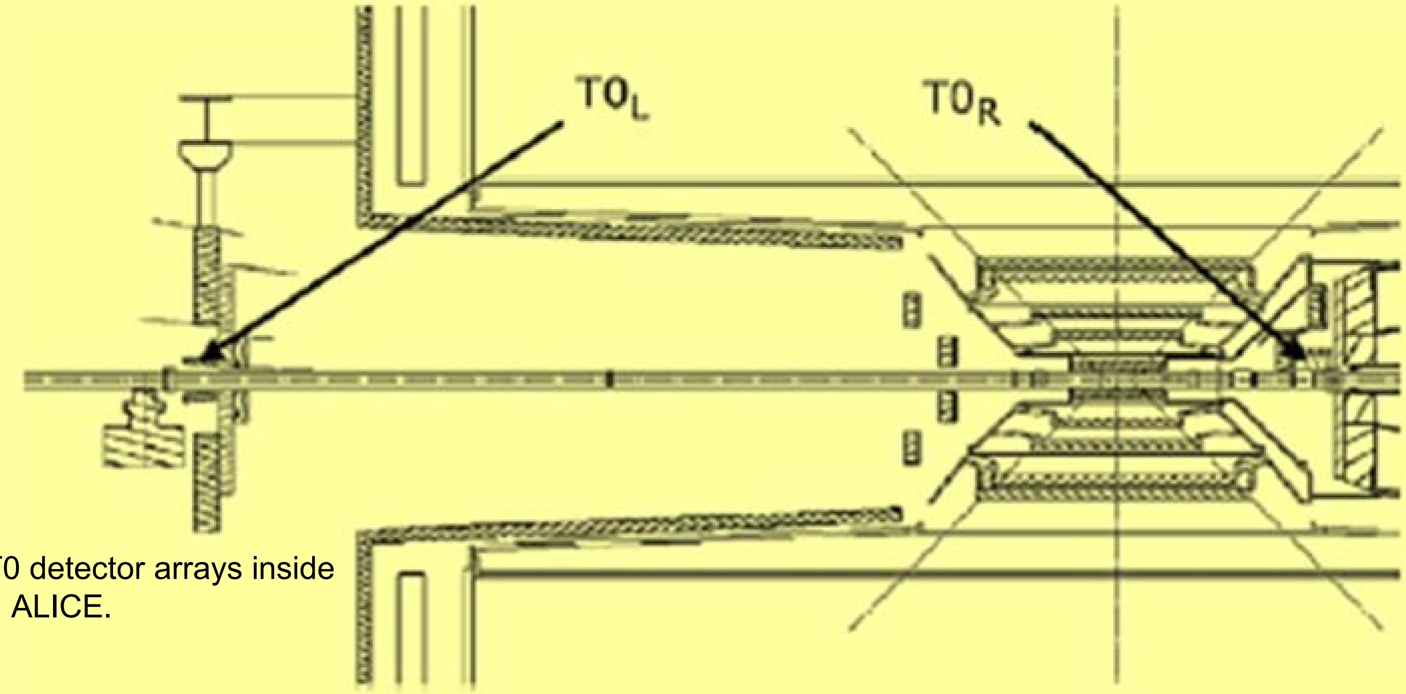

The layout of T0 detector arrays inside ALICE.

Overview of the T0 detector parameters.

Parameters	Left array	Right array
z-position (cm)	−350	+70
Number of Cherenkov counters	12	12
Pseudo-rapidity coverage	$-5 \leqslant \eta \leqslant -4.5$	$2.9 \leqslant \eta \leqslant 3.3$
Detector active area (cm^2)	84.78	84.78
Efficiency with beam pipe (%)	67	60
Efficiency with beam pipe of both arrays in co-incidence (%)	48	
Number of physical readout channels	56	
Time resolution (ps)	37	
Vertex position resolution (cm)	1.3	

Cosmic Ray Trigger Detectors

The Cosmic Ray Trigger (CRT) is a part of ACORDE(A COsmic Ray DEtector for ALICE) which together with some other ALICE tracking detectors, will provide precise information on cosmic rays with primary energies around 10^{15}–10^{17} eV. The CRT system will provide a fast L0 trigger signal to the central trigger processor, when atmospheric muons impinge upon the ALICE detector. The signal will be useful for calibration, alignment and performance of several ALICE tracking detectors, mainly the TPC and ITS. The cosmic-ray trigger signal will be capable to deliver a signal before and during the operation of the LHC beam. The typical rate for single atmospheric muons crossing the ALICE cavern will be less than 3–4Hzm^{-2}

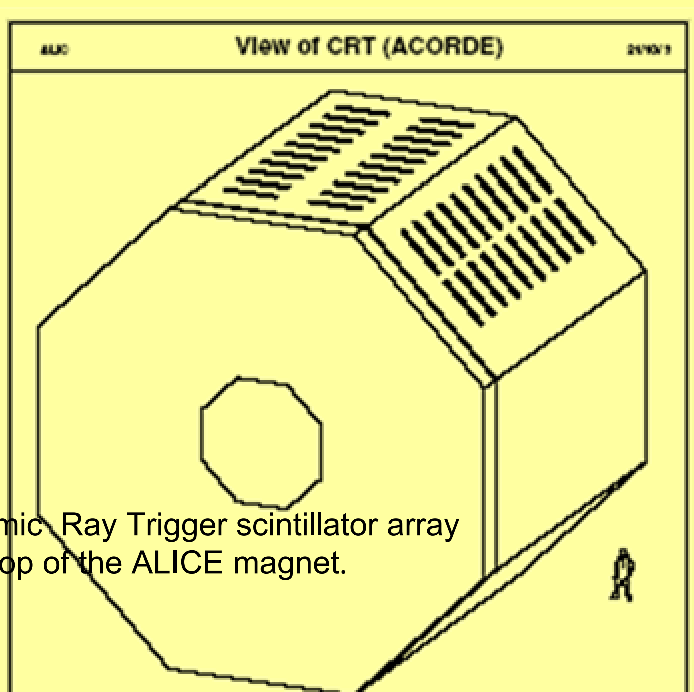

Cosmic Ray Trigger scintillator array on top of the ALICE magnet.

The rate for multi-muon events will be lower (less than 0.04 Hzm^{-2}) but sufficient for the study of these events provided that one can trigger and store tracking information from cosmic muons in parallel to ALICE normal data taking with colliding beams. The energy threshold of cosmic muons arriving to the ALICE hall is approximately 17 GeV, while the upper energy limit for reconstructed muons will be less than 2 TeV, depending of the magnetic field intensity (up to 0.5 T).

Trigger System

The ALICE trigger is designed to select events displaying a variety of different features at rates which can be scaled down to suit physics requirements and the restrictions imposed by the bandwidth of the DAQ and the HLT. The challenge for the ALICE trigger is to make optimum use of the component detectors, which are busy for widely different periods following a valid trigger, and to perform trigger selections in a way which is optimized for several different running modes: ion (Pb–Pb and several lighter species) and pp, having a range of a factor 30 in counting rate.

The first response from the trigger system has to be fast (□1.2 μs) to suit the detector requirements. The principal design requirement for the tracking detectors is to be able to cope with the large multiplicities in Pb–Pb collisions (interaction rate 8 kHz at nominal luminosity). In some cases this requires a strobe to be sent at 1.2 μs. This has led to the requirement that the 'fast' part of the trigger be split into two levels: a L0 signal which reaches detectors at 1.2 μs, but which is too fast to receive all the trigger inputs, and a L1 signal sent at 6.5 μs which picks up all remaining fast inputs.

Another feature of the ALICE environment is that the high multiplicities make events containing more than one central collision unreconstructable. For this reason, past–future protection is an important part of the ALICE trigger. A final level of the trigger L2 waits for the end of the past–future protection interval (88 μs) to verify that the event can be taken. This interval can also be used for running trigger algorithms, though at present there are no candidate algorithms.

Trigger System

List of trigger classes with trigger conditions.

Number	Description	Condition
1	MB	$[\mathrm{T0.V0_{MB}.TRD_{pre}}]_{\mathrm{L0}}[\mathrm{ZDC_1}]_{\mathrm{L1}}$
2	SC	$[\mathrm{T0.V0_{SC}.TRD_{pre}}]_{\mathrm{L0}}[\mathrm{ZDC_2}]_{\mathrm{L1}}$
3	CE	$[\mathrm{T0.V0_{CE}.TRD_{pre}}]_{\mathrm{L0}}[\mathrm{ZDC_3}]_{\mathrm{L1}}$
4	$\mathrm{DM_{unlike,high\,p_T}.TPC.MB}$	$[\mathrm{T0.V0_{MB}.DM_{unlike,high\,p_T}.TRD_{pre}}]_{\mathrm{L0}}[\mathrm{ZDC_1}]_{\mathrm{L1}}$
5	$\mathrm{DM_{unlike,high\,p_T}.TPC.SC}$	$[\mathrm{T0.V0_{SC}.DM_{unlike,high\,p_T}.TRD_{pre}}]_{\mathrm{L0}}[\mathrm{ZDC_2}]_{\mathrm{L1}}$
6	$\mathrm{DM_{unlike,high\,p_T}.No\ TPC.MB}$	$[\mathrm{T0.V0_{MB}.DM_{unlike,high\,p_T}}]_{\mathrm{L0}}[\mathrm{ZDC_1}]_{\mathrm{L1}}$
7	$\mathrm{DM_{unlike,low\,p_T}.No\ TPC.MB}$	$[\mathrm{T0.V0_{MB}.DM_{unlike,low\,p_T}}]_{\mathrm{L0}}[\mathrm{ZDC_1}]_{\mathrm{L1}}$
8	$\mathrm{DM_{unlike,low\,p_T}.No\ TPC.SC}$	$[\mathrm{T0.V0_{SC}.DM_{unlike,low\,p_T}}]_{\mathrm{L0}}[\mathrm{ZDC_2}]_{\mathrm{L1}}$
9	$\mathrm{DM_{like,high\,p_T}.TPC.MB}$	$[\mathrm{T0.V0_{MB}.DM_{like,high\,p_T}.TRD_{pre}}]_{\mathrm{L0}}[\mathrm{ZDC_1}]_{\mathrm{L1}}$
10	$\mathrm{DM_{like,high\,p_T}.TPC.SC}$	$[\mathrm{T0.V0_{SC}.DM_{like,high\,p_T}.TRD_{pre}}]_{\mathrm{L0}}[\mathrm{ZDC_2}]_{\mathrm{L1}}$
11	$\mathrm{DM_{like,high\,p_T}.No\ TPC.MB}$	$[\mathrm{T0.V0_{MB}.DM_{like,high\,p_T}}]_{\mathrm{L0}}[\mathrm{ZDC_1}]_{\mathrm{L1}}$
12	$\mathrm{DM_{like,low\,p_T}.No\ TPC.MB}$	$[\mathrm{T0.V0_{MB}.DM_{like,low\,p_T}}]_{\mathrm{L0}}[\mathrm{ZDC_1}]_{\mathrm{L1}}$
13	$\mathrm{DM_{like,low\,p_T}.No\ TPC.SC}$	$[\mathrm{T0.V0_{SC}.DM_{like,low\,p_T}}]_{\mathrm{L0}}[\mathrm{ZDC_2}]_{\mathrm{L1}}$
14	$\mathrm{DM_{single}.TRD_e.MB}$	$[\mathrm{T0.V0_{MB}.DM_{sl}.TRD_{pre}}]_{\mathrm{L0}}.[\mathrm{TRD_e.ZDC_1}]_{\mathrm{L1}}$
15	$\mathrm{DM_{single}.TRD_e.SC}$	$[\mathrm{T0.V0_{SC}.DM_{sl}.TRD_{pre}}]_{\mathrm{L0}}.[\mathrm{TRD_e.ZDC_2}]_{\mathrm{L1}}$
16	$\mathrm{TRD_e.MB}$	$[\mathrm{T0.V0_{MB}.TRD_{pre}}]_{\mathrm{L0}}.[\mathrm{TRD_e.ZDC_1}]_{\mathrm{L1}}$
17	$\mathrm{TRD_{low\,p_T}.MB}$	$[\mathrm{T0.V0_{MB}.TRD_{pre}}]_{\mathrm{L0}}.[\mathrm{TRD_{low\,p_T}.ZDC_1}]_{\mathrm{L1}}$
18	$\mathrm{TRD_{high\,p_T}.MB}$	$[\mathrm{T0.V0_{MB}.TRD_{pre}}]_{\mathrm{L0}}.[\mathrm{TRD_{high\,p_T}.ZDC_1}]_{\mathrm{L1}}$
19	$\mathrm{TRD_{unlike,high\,p_T}.MB}$	$[\mathrm{T0.V0_{MB}.TRD_{pre}}]_{\mathrm{L0}}.[\mathrm{TRD_{unlike,high\,p_T}.ZDC_1}]_{\mathrm{L1}}$
20	$\mathrm{TRD_{unlike,high\,p_T}.SC}$	$[\mathrm{T0.V0_{SC}.TRD_{pre}}]_{\mathrm{L0}}.[\mathrm{TRD_{unlike,high\,p_T}.ZDC_2}]_{\mathrm{L1}}$
21	$\mathrm{TRD_{like,high\,p_T}.MB}$	$[\mathrm{T0.V0_{MB}.TRD_{pre}}]_{\mathrm{L0}}.[\mathrm{TRD_{like,high\,p_T}.ZDC_1}]_{\mathrm{L1}}$
22	$\mathrm{TRD_{like,high\,p_T}.SC}$	$[\mathrm{T0.V0_{SC}.TRD_{pre}}]_{\mathrm{L0}}.[\mathrm{TRD_{like,high\,p_T}.ZDC_2}]_{\mathrm{L1}}$
23	$\mathrm{TRD_{jet,high\,p_T}.SC}$	$[\mathrm{T0.V0_{SC}.TRD_{pre}}]_{\mathrm{L0}}.[\mathrm{TRD_{jet,high\,p_T}.ZDC_1}]_{\mathrm{L1}}$
24	$\mathrm{TRD_{jet,low\,p_T}.MB}$	$[\mathrm{T0.V0_{MB}.TRD_{pre}}]_{\mathrm{L0}}.[\mathrm{TRD_{jet,low\,p_T}.ZDC_1}]_{\mathrm{L1}}$
25	$\mathrm{TRD_{jet,low\,p_T}.SC}$	$[\mathrm{T0.V0_{SC}.TRD_{pre}}]_{\mathrm{L0}}.[\mathrm{TRD_{jet,low\,p_T}.ZDC_2}]_{\mathrm{L1}}$
26	$\mathrm{PHOS_{high\,p_T}.MB}$	$[\mathrm{T0.V0_{MB}.PHOS_{high\,p_T}.TRD_{pre}}]_{\mathrm{L0}}[\mathrm{ZDC_1}]_{\mathrm{L1}}$
27	$\mathrm{PHOS_{low\,p_T}.MB}$	$[\mathrm{T0.V0_{MB}.PHOS_{low\,p_T}.TRD_{pre}}]_{\mathrm{L0}}[\mathrm{ZDC_1}]_{\mathrm{L1}}$
28	$\mathrm{PHOS_{low\,p_T}.SC}$	$[\mathrm{T0.V0_{SC}.PHOS_{low\,p_T}.TRD_{pre}}]_{\mathrm{L0}}[\mathrm{ZDC_2}]_{\mathrm{L1}}$
29	PHOS Standalone	$[\mathrm{T0.V0_{MB}.PHOS_{MB}}]_{\mathrm{L0}}[\mathrm{ZDC_1}]_{\mathrm{L1}}$
30	$\mathrm{EMCAL_{jet,high_T}.MB}$	$[\mathrm{T0.V0_{MB}.EMCAL_{jet,high\,p_T}}]_{\mathrm{L0}}[\mathrm{ZDC_1}]_{\mathrm{L1}}$
31	$\mathrm{EMCAL_{jet,med\,p_T}.MB}$	$[\mathrm{T0.V0_{MB}.EMCAL_{jet,med\,p_T}}]_{\mathrm{L0}}[\mathrm{ZDC_1}]_{\mathrm{L1}}$
32	$\mathrm{EMCAL_{jet,low\,p_T}.MB}$	$[\mathrm{T0.V0_{MB}.EMCAL_{jet,low\,p_T}}]_{\mathrm{L0}}[\mathrm{ZDC_1}]_{\mathrm{L1}}$
33	$\mathrm{EMCAL_{jet,low\,p_T}.SC}$	$[\mathrm{T0.V0_{SC}.EMCAL_{jet,low\,p_T}}]_{\mathrm{L0}}[\mathrm{ZDC_2}]_{\mathrm{L1}}$
34	$\mathrm{ZDC_{dis}}$	$[\mathrm{BX}]_{\mathrm{L0}}.[\mathrm{ZDC_{spe}}]_{\mathrm{L1}}$
35	cosmic	$[\mathrm{BX.cosmic\_telescope}]_{\mathrm{L0}}$
36	beam gas	$[\mathrm{T0_{beamgas}}]_{\mathrm{L0}}$

List of trigger inputs for Pb–Pb and pp interactions.

Number	L0 (Pb–Pb)	L0 (pp)	L1 (Pb–Pb)
1	V0 minimum bias	V0 minimum bias	TRD unlike e pair high p_T
2	V0 semi-central	V0 high multiplicity	TRD like e pair high p_T
3	V0 central	V0 beam gas	TRD jet low p_T
4	V0 beam gas	T0 right	TRD jet high p_T
5	T0 vertex	T0 left	TRD electron
6	PHOS MB	T0 vertex	TRD hadron low p_T
7	PHOS jet low p_T	PHOS MB	TRD hadron high p_T
8	PHOS jet high p_T	PHOS jet low p_T	ZDC 1
9	EMCAL MB	PHOS jet high p_T	ZDC 2
10	EMCAL jet high p_T	EMCAL MB	ZDC 3
11	EMCAL jet med p_T	EMCAL jet high p_T	ZDC special
12	EMCAL jet low p_T	EMCAL jet med p_T	Topological 1
13	Cosmic Telescope	EMCAL jet low p_T	Topological 2
14	DM like high p_T	Cosmic Telescope	
15	DM unlike high p_T	DM like high p_T	
16	DM like low p_T	DM unlike high p_T	
17	DM unlike low p_T	DM like low p_T	
18	DM single	DM unlike low p_T	
19	TRD pre-trigger	DM single	
20		TRD pre-trigger	

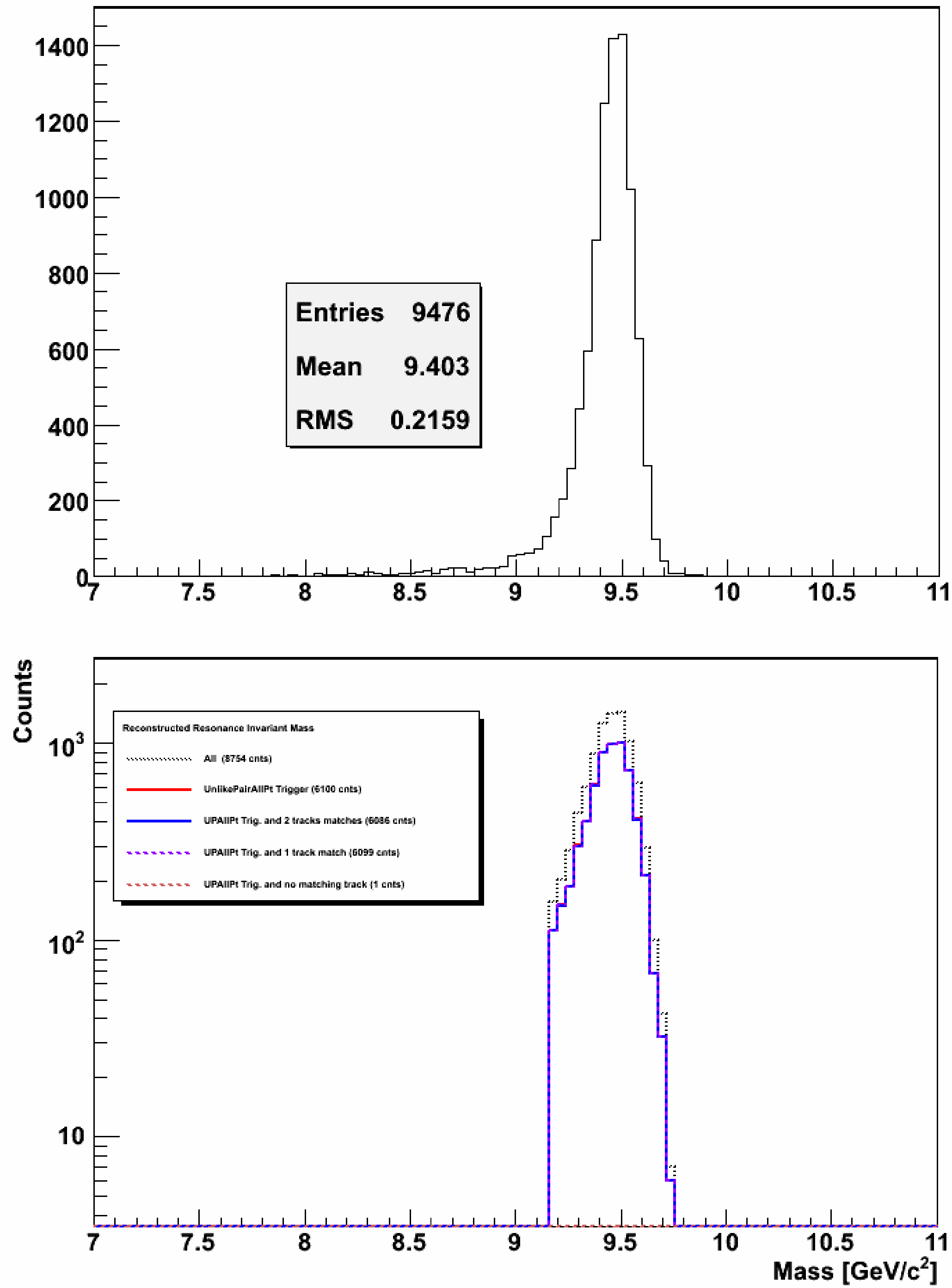

Entries 9476
Mean 9.403
RMS 0.2159
0
200
400
600
800
1000
1200
1400
7
7.5
8
8.5
9
9.5
10
10.5
11
Counts
Reconstructed Resonance Invariant Mass
All (8754 cnts)
UnlikePairAllPt Trigger (6100 cnts)
UPAllPt Trig. and 2 tracks matches (6086 cnts)
UPAllPt Trig. and 1 track match (6099 cnts)
UPAllPt Trig. and no matching track (1 cnts)
10
10^2
10^3
Mass [GeV/c^2]